

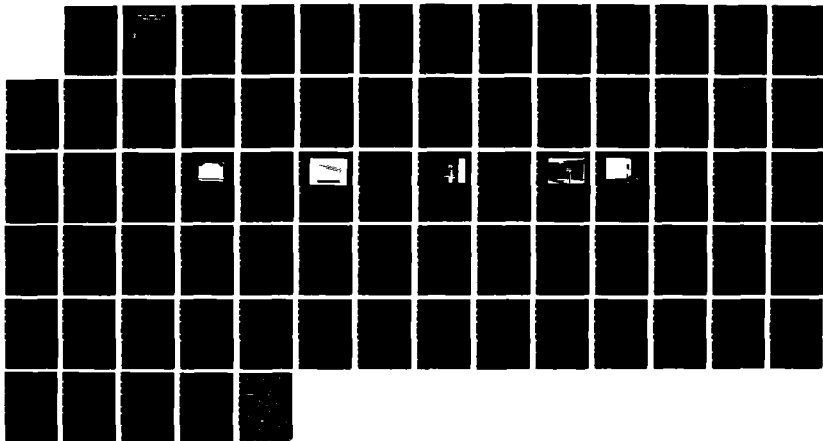
AD-A192 408

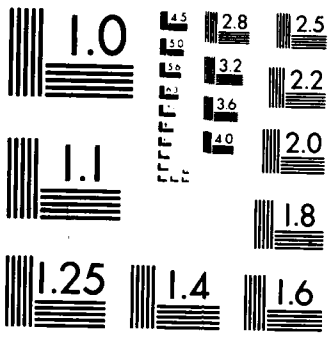
THE EFFECT OF A TURBULENT AIRSTREAM ON A
VERTICALLY-LAUNCHED MISSILE AT HIGH ANGLES OF ATTACK
(U) NAVAL POSTGRADUATE SCHOOL MONTEREY CA D P ROANE
DEC 87 F/G 16/2

1/1

UNCLASSIFIED

NL





AD-A192 408

NAVAL POSTGRADUATE SCHOOL Monterey, California



S DTIC
ELECTE
MAY 12 1988
D

THESIS

THE EFFECT OF A TURBULENT AIRSTREAM
ON A VERTICALLY-LAUNCHED MISSILE
AT HIGH ANGLES OF ATTACK

by

Donald P. Roane, Jr.

December 1987

Thesis Advisor

Richard M. Howard

Approved for public release; distribution is unlimited.

UNCLASSIFIED

SECURITY CLASSIFICATION OF THIS PAGE

REPORT DOCUMENTATION PAGE

A192 408

1a. REPORT SECURITY CLASSIFICATION UNCLASSIFIED			1b. RESTRICTIVE MARKINGS N/A	
2a. SECURITY CLASSIFICATION AUTHORITY N/A			3. DISTRIBUTION / AVAILABILITY OF REPORT Approved for public release; Distribution unlimited.	
2b. DECLASSIFICATION / DOWNGRADING SCHEDULE N/A			4. PERFORMING ORGANIZATION REPORT NUMBER(S)	
4. PERFORMING ORGANIZATION REPORT NUMBER(S)			5. MONITORING ORGANIZATION REPORT NUMBER(S)	
6a. NAME OF PERFORMING ORGANIZATION Naval Postgraduate School		6b. OFFICE SYMBOL (if applicable) Code 33	7a. NAME OF MONITORING ORGANIZATION Naval Postgraduate School	
6c. ADDRESS (City, State, and ZIP Code) Monterey, California 93943-5100			7b. ADDRESS (City, State, and ZIP Code) Monterey, California 93943-5100	
8a. NAME OF FUNDING, SPONSORING ORGANIZATION		8b. OFFICE SYMBOL (if applicable)	9. PROCUREMENT INSTRUMENT IDENTIFICATION NUMBER	
8c. ADDRESS (City, State, and ZIP Code)			10. SOURCE OF FUNDING NUMBERS	
			PROGRAM ELEMENT NO.	PROJECT NO.
			TASK NO.	WORK UNIT ACCESSION NO.
11. TITLE (Include Security Classification) THE EFFECT OF A TURBULENT AIRSTREAM ON A VERTICALLY-LAUNCHED MISSILE AT HIGH ANGLES OF ATTACK				
12. PERSONAL AUTHOR(S) Roane, Donald P. (Jr.)				
13a. TYPE OF REPORT Master's Thesis		13b. TIME COVERED FROM _____ TO _____	14. DATE OF REPORT (Year, Month, Day) 1987 December	15. PAGE COUNT 72
16. SUPPLEMENTARY NOTATION				
17. COSATI CODES			18. SUBJECT TERMS (Continue on reverse if necessary and identify by block number)	
FIELD	GROUP	SUB-GROUP	Vertical Launch, Missile, Turbulence, High Angle, of Attack, Vortices ←	
19. ABSTRACT (Continue on reverse if necessary and identify by block number) The purpose of this thesis is to initiate an investigation of the response of a shipboard surface-to-air missile launched vertically into a region of turbulence at high angles of attack. A review was conducted on the effects of asymmetric vortices, turbulent flowfields, and the marine atmospheric environment on a slender body of revolution. Turbulence mapping of a wind tunnel with installed turbulence-generating grids was conducted using hot-wire anemometry. The resultant turbulence intensities and length scales were analyzed as a function of the downstream distance and the grid mesh-width/bar-diameter ratio. Turbulence intensity was found to decrease, while the length scale increased, with increasing distance from the generating grid. Both the turbulence intensity and length scale increased with an increase in the grid bar diameter. A generic, vertically-launched surface-to-air				
20. DISTRIBUTION / AVAILABILITY OF ABSTRACT <input checked="" type="checkbox"/> UNCLASSIFIED/UNLIMITED <input type="checkbox"/> SAME AS RPT <input type="checkbox"/> DTIC USERS			21. ABSTRACT SECURITY CLASSIFICATION UNCLASSIFIED	
22a. NAME OF RESPONSIBLE INDIVIDUAL Richard M. Howard			22b. TELEPHONE (Include Area Code) (408)-646-2870	22c. OFFICE SYMBOL Code 67Ho

DD FORM 1473, 84 MAR

83 APR edition may be used until exhausted.
All other editions are obsolete

SECURITY CLASSIFICATION OF THIS PAGE

U.S. Government Printing Office: 1986-608-243

UNCLASSIFIED

1
> keywords:

Item 19. - continued

missile (VLSAM) model was developed and constructed for further wind tunnel testing, to include force, moment, pressure and flow visualization studies.

Accession For	
NTIS CRA&I	<input checked="" type="checkbox"/>
DTIC TAB	<input type="checkbox"/>
Unannounced	<input type="checkbox"/>
Justification	
By	
Distribution/	
Availability Codes	
Dist	Avail and/or Special
A-1	



Approved for public release; distribution is unlimited.

The Effect of a Turbulent Airstream
on a Vertically-Launched Missile
at High Angles of Attack

by

Donald P. Roane, Jr.
Lieutenant, United States Navy
B.S., United States Naval Academy, 1981

Submitted in partial fulfillment of the
requirements for the degree of

MASTER OF SCIENCE IN ENGINEERING SCIENCE

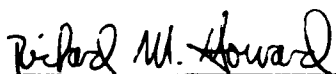
from the

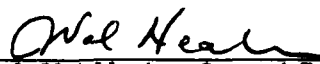
NAVAL POSTGRADUATE SCHOOL
December 1987

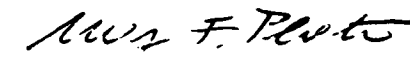
Author:


Donald P. Roane, Jr.

Approved by:


Richard M. Howard, Thesis Advisor


J. Val Healey, Second Reader


Max F. Platzer, Chairman.
Department of Aeronautics


Gordon E. Schacher,
Dean of Science and Engineering

ABSTRACT

The purpose of this thesis is to initiate an investigation of the response of a shipboard surface-to-air missile launched vertically into a region of turbulence at high angles of attack. A review was conducted on the effects of asymmetric vortices, turbulent flowfields, and the marine atmospheric environment on a slender body of revolution. Turbulence mapping of a wind tunnel with installed turbulence-generating grids was conducted using hot-wire anemometry. The resultant turbulence intensities and length scales were analyzed as a function of the downstream distance and the grid mesh-width bar-diameter ratio. Turbulence intensity was found to decrease, while the length scale increased, with increasing distance from the generating grid. Both the turbulence intensity and length scale increased with an increase in the grid bar diameter. A generic, vertically-launched surface-to-air missile (VLSAM) model was developed and constructed for further wind tunnel testing, to include force, moment, pressure and flow visualization studies.

TABLE OF CONTENTS

I.	INTRODUCTION	12
A.	BACKGROUND	12
1.	Asymmetric Vortex Theory	13
B.	TURBULENCE	17
1.	Turbulence Intensity and Length Scale	17
2.	Boundary Layer Effects	19
3.	Marine Environment	19
4.	Mach and Reynolds Number Effects	20
C.	EFFECTS ON VERTICALLY-LAUNCHED SURFACE- TO-AIR MISSILES	21
1.	Launch and Crosswind Velocities	22
2.	Other Launch Considerations	23
II.	EQUIPMENT AND PROCEDURES	26
A.	APPARATUS	26
1.	Wind Tunnel	26
2.	Turbulence Grids	27
3.	Missile Model and Support System	29
4.	Hot-Wire Anemometry Equipment	31
B.	PROCEDURE	34
1.	Hot-Wire Calibration	34
2.	Turbulence Mapping	36
III.	RESULTS	39
A.	HOT-WIRE ANEMOMETRY	39
1.	Hot-Wire Calibration	39
2.	Turbulence Mapping	39
IV.	CONCLUSIONS AND RECOMMENDATIONS	51

APPENDIX A: HOT-WIRE CALIBRATION COMPUTER PROGRAM	53
APPENDIX B: TURBULENCE MAPPING RESULTS	64
LIST OF REFERENCES	69
INITIAL DISTRIBUTION LIST	71

LIST OF TABLES

1. GENERIC VLSAM LAUNCH VELOCITY HISTORY	22
2. GRID SPECIFICATIONS	28
3. HOT-WIRE SENSOR LOCATION	37
4. HOT-WIRE CALIBRATION RESULTS	40
5. TURBULENCE DATA FOR GRID #1	42
6. TURBULENCE DATA FOR GRID #2	42
7. TURBULENCE DATA FOR GRID #3	43
8. TURBULENCE DATA FOR GRID #4	43
9. GRID-GENERATED TURBULENCE INTENSITIES	45
10. GRID-GENERATED LENGTH SCALES	48

LIST OF FIGURES

1.1	Vortex Flow About an Unyawed Blunt-Nosed Cylinder	14
1.2	Vortex Flow About an Unyawed Slender-Nose Cylinder	15
1.3	Vortex Shedding on a Body at High Angles of Attack (see Reference 6)	16
1.4	Generic VLSAM Launch Velocity versus Time	23
1.5	Resultant Missile Velocity Vector	24
2.1	Schematic of Wind Tunnel	27
2.2	Position of Turbulence Grids in Wind Tunnel	28
2.3	Turbulence-Generating Grid Mounted in Wind Tunnel	29
2.4	Square-Mesh Turbulence-Generating Grid	30
2.5	VLSAM Missile Model	31
2.6	Block Diagram of Hot-Wire Calibration Apparatus	32
2.7	Hot-Wire Sensor and Pressure Probes	33
2.8	Block Diagram of Turbulence Mapping Apparatus	34
2.9	Hot-Wire Sensor Mounted For Turbulence Mapping	35
2.10	Hot-Wire Sensor Downstream of Turbulence Grid	36
3.1	Hot-Wire Calibration Results	41
3.2	Grid-Generated Turbulence Intensity Curves	46
3.3	Turbulence Intensity at Position 0 in Wind Tunnel	47
3.4	Grid-Generated Length Scale Curves	49
3.5	Turbulence Length Scale at Position 0 in Wind Tunnel	50
B.1	Turbulence Intensities and Length Scales For Grid #1	65
B.2	Turbulence Intensities and Length Scales For Grid #2	66
B.3	Turbulence Intensities and Length Scales For Grid #3	67
B.4	Turbulence Intensities and Length Scales For Grid #4	68

NOMENCLATURE

a_z	acceleration in z-direction
C_f	skin friction coefficient
d	reference diameter
L_e	dissipation length scale
M	Mach number
N	normal force
P'	rms of velocity fluctuation ($= \sqrt{\overline{u^2} + \overline{v^2}}$)
rms	root-mean-square
R	operating resistance
Re	Reynolds number ($= (\rho U d) / \mu$)
R_{tot}	probe resistance
R_{20}	sensor resistance at 20° C
t	time
T_o	ambient temperature
T_s	selected sensor operating temperature
T_u	turbulence intensity ($= u'/U$)
u	longitudinal velocity fluctuation
u'	rms of u ($= \sqrt{\overline{u^2}}$)
U	longitudinal mean velocity
v	lateral velocity fluctuation
v'	rms of v ($= \sqrt{\overline{v^2}}$)
V_l	launch velocity
V_c	crosswind velocity
V_r	resultant velocity
Y	side force
z	altitude
z_i	launcher elevation
z_o	roughness length
α	angle of attack
α_{20}	temperature coefficient of sensor resistance at 20° C
δ	boundary layer thickness

δ_n nose semi-vertex angle
 θ_a asymmetric vortex onset angle
 μ absolute viscosity
 ρ density

ACKNOWLEDGEMENT

The assistance of the Navy-NASA Joint Institute of Aeronautics is gratefully acknowledged. In particular, the support provided by the following individuals is recognized:

- Mr. Jack Brownson, Aerodynamic Facilities Branch, NASA-Ames Research Facility
- Mr. Jim McMahon, Balance Calibration Laboratory, NASA-Ames Research Facility

I. INTRODUCTION

A. BACKGROUND

The recent introduction of a vertical launcher capability for ships carrying surface-to-air missiles represents a major advancement in weapon system reliability and flexibility. Conventional trainable launcher systems are extremely vulnerable to mechanical failure: in such instances, a fully loaded missile magazine is rendered useless. However, each vertically-launched missile is fired from its own storage container, effectively increasing the redundancy of the launcher systems. Additionally, a vertical launcher system has unimpeded access to any of the weapons in the magazine; conventional launchers require cycling of the weapons until the desired round is in position for launch.

The development of these new launcher systems, however, also creates problems not previously encountered with conventionally trained launchers. Launching a missile vertically into the open ocean environment exposes the missile, while still at low launch velocity, to potentially significant crosswinds. The result is a missile flying at relatively low velocities at an effective high angle of attack. Under such conditions, largely unpredictable side forces can be generated, which pose a serious threat to flight stability.

Additionally, the airstream close to the ocean surface and over the deck of the launching platform may be relatively turbulent. In determining the effect of turbulence on boundary layer development, both the turbulence intensity and turbulence length scale must be considered. In the marine atmospheric boundary layer, the turbulence intensity may be relatively high; values as high as 12 to 17 percent are possible. Additionally, large scale turbulence (of a scale comparable to the dimension of the affected body) is present in marine environment. Large-scale turbulence has been shown to be a primary cause for the rolling, pitching and yawing motion of bodies subjected to such an environment. On the other hand, the degree to which high intensity small-scale turbulence is present in the atmosphere, and the consequent effect it has on missile boundary layer development, is largely unknown. [Ref. 1: pp. 3, 34]

The characteristics of out-of-plane forces and moments on unyawed slender bodies of revolution at high angles of attack, caused largely by asymmetric vortex

shedding, have been investigated for over three decades (see Reference 2). Much of the research to date has attempted to model or predict the flow about such bodies and to examine the effect of design changes on the observed flow. Experimentally, several methods have been employed to analyze both the cause and effect of these asymmetric vortices. These methods include direct measurement of forces and moments, pressure measurements, and flow visualization. Force moment measurements permit an analysis of the magnitude of the disturbances, while pressure distributions and flow visualization enable the observer to study the location and development of the asymmetric vortices.

The goal of this thesis is to research and experimentally study the aerodynamic characteristics of a generic, vertically-launched surface-to-air missile (VLSAM) in a turbulent airstream at high angles of attack. Although extensive research and experimental work has been conducted by the author in the development of this thesis, it is not a conclusive study of the problem outlined above. Further experimental work will be conducted at the Naval Postgraduate School in a continuing effort to understand the effects of turbulence on slender bodies at high angles of attack.

1. Asymmetric Vortex Theory

The flow about a pitched, unyawed blunt-nosed slender cylindrical body can be characterized in part as being similar to the flow behind a two-dimensional cylinder at an angle of attack to the flowfield. As shown in Figure 1.1, a separation "bubble" exists at the nose of the body. Further down the length of the cylinder, two symmetrically disposed vortices begin to form on the lee side. These vortices are fed by the vortex sheets of boundary layer fluid which have separated from the body. Further along the length of the body these vortices alternate in their separation from the surface. The result is a side force on the body, relatively small in magnitude, which appears as a consequence of the steady asymmetric vortices. The description above assumed a blunt-nosed cylinder. In this instance, a nose-induced flow separation will occur which prevents the formation of vortices in the area immediately aft of the nose. [Ref. 3: pp. 751-752]

With the addition of a slender ogive nose, the blunt-nose induced separation will not occur. Consequently, large asymmetric vortices now appear at the nose of the body. The aft portion of the cylinder will still produce a side force as described above, but the magnitude of that produced by the nose is a much greater proportion of the overall side force. The net effect is that of a slender body with vortex formation now occurring along the entire length of the body, as shown in Figure 1.2. [Ref. 4: p. 99]

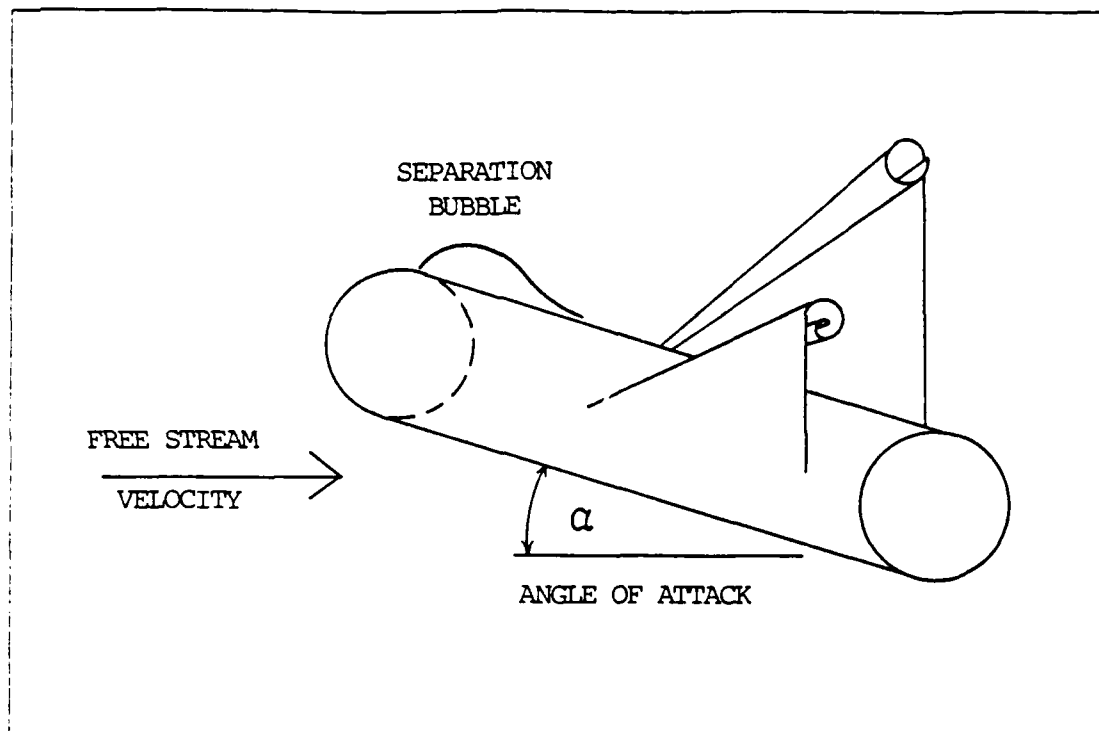


Figure 1.1 Vortex Flow About an Unyawed Blunt-Nosed Cylinder.

The point at which the transition from symmetric to asymmetric vortex shedding begins is dependent on several factors, notably the body length, the nose cone apex angle, the angle of attack, the flow Mach number, and the Reynolds number. (The effects of the Mach and the Reynolds number will be covered in the following section.) The transition can actually be divided into four separate regions, as shown in Figure 1.3. Each of these regions can be described by the angle of attack α and characterized by the type of flow present (see Reference 5 pp. 22-23). Regime I ($0^\circ < \alpha < 5^\circ$) represents a classical potential flowfield with no flow separation. Regime II ($5^\circ < \alpha < 20^\circ$) shows flow separation in the form of two symmetric vortices on the lee side of the body: no side forces or yawing moments are induced. In Regime III ($20^\circ < \alpha < 60^\circ$), the vortices are now shed asymmetrically. This effect produces both side forces and yawing moments. Regime IV ($60^\circ < \alpha < 90^\circ$) resembles wake-like flow in the region behind a two-dimensional cylinder. (The angles given are approximate and do not necessarily represent the actual points of transition.)

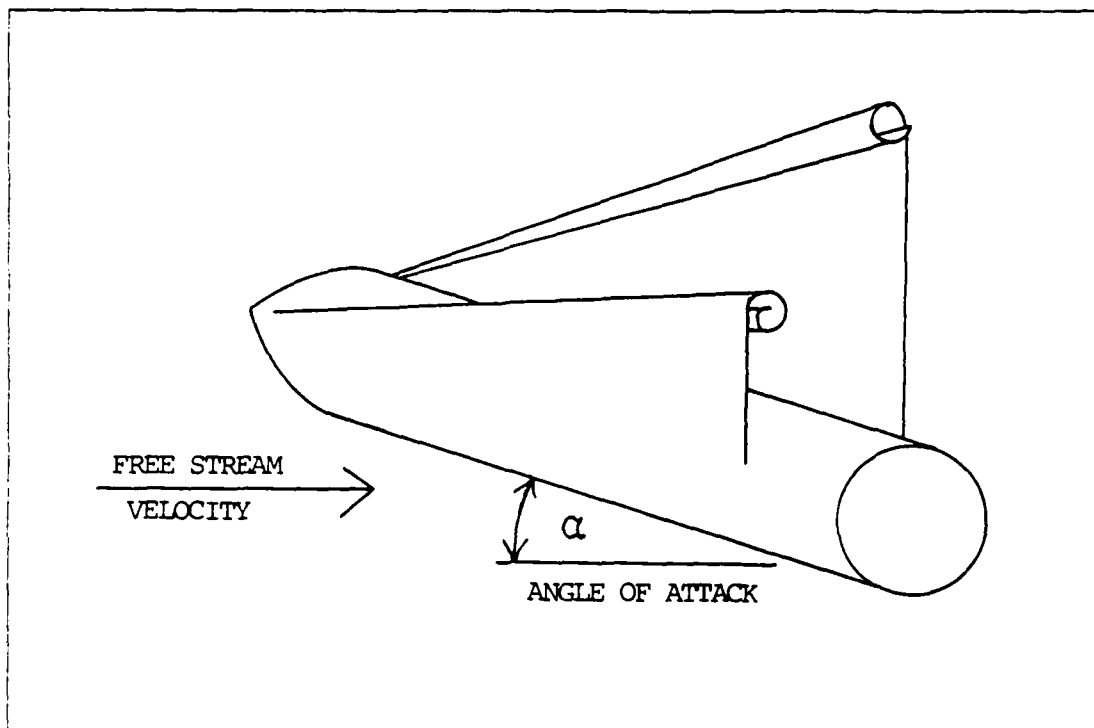


Figure 1.2 Vortex Flow About an Unyawed Slender-Nose Cylinder.

On a slender cylinder with a relatively fine tapered nose in a subsonic, low turbulence (T_u less than one percent) flow, asymmetric vortex shedding usually appears at an angle θ_a , when the angle of attack α is approximately twice the nose semi-vertex angle δ_n . As the angle of attack is increased above the angle θ_a , the region of symmetrical wake decreases and the asymmetric flow pattern predominates. The result of this increasing tendency toward asymmetric flow is the appearance of out-of-plane forces and moments. Steady or unsteady asymmetric vortex shedding, or "flow switching," can occur as the angle of attack increases. Steady asymmetric vortex shedding produces a side force Y which increases to some maximum with increasing angle of attack. The magnitude of the side force then decreases as the angle of attack is increased. As the angle of attack is increased still further, steady vortex shedding gives way to high frequency unsteady shedding, and the side forces disappear. [Ref. 7: pp. 1-5]

Detailed descriptions of specific experimental results were intentionally neglected in the above descriptions. The behavior of the asymmetric vortices is well documented for a vast number of models and shapes, yet their cause is still not

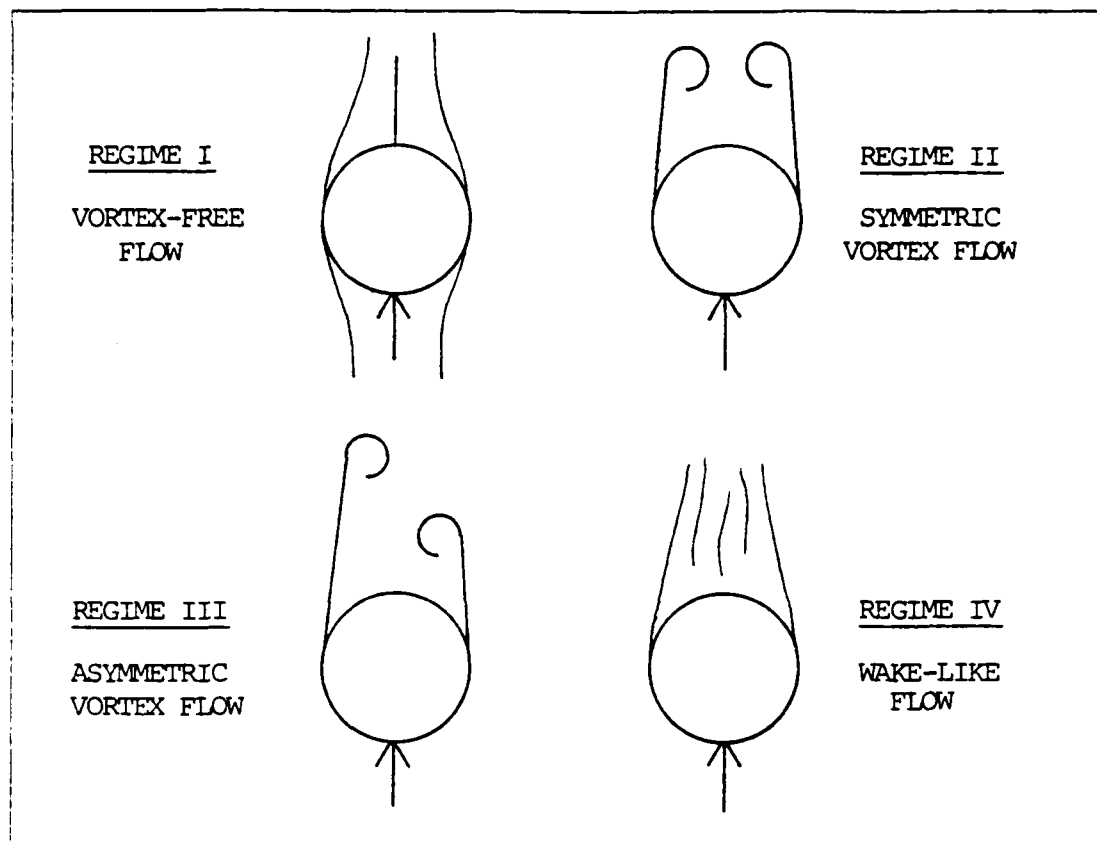


Figure 1.3 Vortex Shedding on a Body at High Angles of Attack
(see Reference 6).

positively established. Most theories suggest a relationship between the flow separation along the body and an inviscid interaction of the vortices [Ref. 8: pp. 2-3]. A prominent theory, put forth by Keener and Chapman, is that minute variations or disturbances at the nose apex lead to the formation of asymmetric vortices [Ref. 7: pp. 2-3].

Several important generalizations can be made regarding the effect of configurational changes on experimental results. The addition of a long cylindrical afterbody, as well as decreasing the nose apex angle, will result in a decrease in the asymmetric vortex onset angle θ_a [Ref. 7: p. 5]. The placement of long strakes along the missile body and nose was found to reduce the forces and moments generated by asymmetric vortices [Ref. 6: pp. 5-7]. The use of small nose bluntness, nose booms and boundary layer trips has also proven effective in reducing asymmetric vortex-induced

loads [Ref. 9: p. 552]. Other methods are available for reducing the formation of asymmetric vortices. Those listed above, however, are relatively simple to implement, both in design and experimental work. While these methods have generally resulted in a reduction of vortex generated side forces, they do not necessarily work in combination, nor do they always give consistent results, even under similar test conditions. Additionally, the effect of the changes may adversely affect some other areas of concern, such as lift, drag, or stability.

B. TURBULENCE

The term *turbulence* is best characterized by the presence of random, short-duration, small-scale variations in a flowfield with a given mean velocity. In calculating the effect of turbulence on a body in the flowfield, a comparison must be made between the scale of the body and that of the turbulence. In addition, consideration must be given to the energy contained in the turbulent flowfield.

1. Turbulence Intensity and Length Scale

The turbulence intensity, T_u , is defined as the ratio of the root-mean-square (rms) value of the fluctuating streamwise velocity component to the mean velocity component in a flowfield. Mathematically presented as Equation 1.1,

$$T_u = u'/U \quad (\text{eqn 1.1})$$

the turbulence intensity gives a measure of the relative magnitude of the velocity fluctuations. The turbulence intensity also yields an indication of the kinetic energy of the turbulence, via the term u' in Equation 1.1. Therefore, high turbulence intensity correlates to high kinetic energy in the velocity fluctuations, i.e. more "turbulent" flow.

The length scale of the turbulence is a measure of the dimension of the velocity fluctuation. The effect of the length scale on a body is a function of the relative dimensions of the turbulent eddies and the body itself. The length scale, despite the inference of a purely spatial measure, also represents the temporal character of the turbulent fluctuations. An increase in the spatial length of the turbulence corresponds to an increase in the time the body is exposed to the fluctuation.

The dimension of the length scale relative to a body can be regarded in three broad categories; larger than the body, equal to the body, and smaller than the body.

For turbulent eddies of a scale much larger than the body, the effect is similar to that experienced in the non-turbulent flowfield, where the deviations in the speed and direction would be of long duration. Thus, the motion of the body would be affected in the same manner as one in which the flowfield had changed for a long period of time. In contrast, the unwanted rolling, pitching, and yawing motion of the body is caused primarily by turbulent fluctuations of a scale comparable to the dimensions of that body [Ref. 1: p. 3]. Both of these instances are similar in that the turbulence length scales impact the motion of the whole body.

Length scales of a dimension much smaller than the body, however, have a distinctly different effect. These length scales have a magnitude comparable to the thickness of the boundary layer on the surface of the body. Therefore, the effect of small-scale turbulence is on the flow over the surface of the body. The development of a boundary layer and flow separation over the body can thus be greatly affected by such relatively small-scale turbulence.

The length scale of a given velocity fluctuation, subject to interaction with other fluctuations in the turbulent flowfield, is not constant. As described by Bradshaw (see Reference 10), the effect of vortex stretching tends to decrease the length scale of turbulent eddies. This "cascade" effect is caused by a strain in one direction affecting the orthogonal components due to the conservation of angular momentum. For example, consider a vortex rotating in an x-y plane. Strain applied in the z direction causes an increase in the velocity and a decrease in the length scales of both the x and y components. The increase in the x and y velocity components then similarly affects the velocity and length scales of the y-z and x-z components, respectively. The "cascade" continues to decrease the scale of the eddies, until the energy contained therein is finally dissipated due to viscosity. [Ref. 10: pp. 14-15]

The cascade effect therefore produces, from a single source, eddies of various length scales. At any point in time, turbulence may be characterized by a representative, or "average", length scale. For turbulence generated at a single source, the representative length scale may be relatively small due to the transfer of energy from large to small eddies via cascading. However, as the turbulence decays, the energy transfer also decreases. This causes the intensity of the smaller eddies to decrease faster than the larger eddies. Thus, despite the formation of smaller eddies by cascading, larger eddies predominate; as the smaller eddies disappear due to viscosity, the dissipation rate decreases and the representative length scale increases. [Ref. 10: p. 48]

2. Boundary Layer Effects

In view of the fact that small-scale turbulent length scales can affect the missile boundary layer development, the effects of such interactions should be reviewed. An important factor to be considered is the point at which asymmetric vortices begin to form. More significant, however, is the point at which any type of flow separation occurs, be it symmetric or asymmetric. Delaying all types of flow separation will inevitably decrease the tendency toward the formation of asymmetric vortices.

A dimensionless parameter useful in analyzing the boundary layer effects is the skin friction coefficient, C_f . In general, a fluid which is moving over a relatively smooth surface (low C_f) will experience flow separation sooner than would the same flow moving over a rough surface. This is a result of the turbulent flow close to the rough surface. Such a boundary layer will resist separation longer due to the high kinetic energy which reduces the tendency toward flow deceleration at that point. Therefore, increasing C_f generally delays the onset of flow separation.

Experimental data presented by Hancock and Bradshaw (see Reference 11) and Meier and Kreplin (see Reference 12) show an inverse relationship between turbulence length scales and the skin friction coefficient; as the length scale is decreased, C_f increases. More specifically, the maximum value of the skin friction coefficient occurs when the length scale is on the order of the boundary layer thickness δ . Both of these experiments used turbulence grids in wind tunnels, which ideally generate isotropic homogeneous turbulence at a large distance from the plane of the grid [Ref. 10: p. 48].

Thus, as the ratio of dissipation length scale to boundary layer thickness (L_e/δ) approaches unity, the onset of flow separation is delayed. In other words, the presence of small-scale turbulence (of a dimension comparable to the boundary layer) decreases the tendency to form asymmetric vortices.

3. Marine Environment

The atmospheric boundary layer into which the vertically launched surface-to-air missile (VLSAM) is launched is best described as turbulent [Ref. 13: p. 51]. In general, the turbulence fluctuations are greater over land than over sea. However, the characteristics of turbulence in the marine environment are not fully understood, and the effects on missile boundary layer development deserve investigation.

The atmospheric boundary layer (ABL) is formed by the interaction of the atmosphere and the surface (land or sea) over which it flows. Turbulence in this region is caused by a transfer of heat, momentum, and mass. The lowest segment of the ABL, termed the surface layer, is characterized by mechanically produced turbulence resulting from surface roughness. The surface layer comprises the lower ten percent of the ABL, and is on the order of 50 meters in height. Furthermore, the majority of the flow in the surface layer itself can be considered horizontally homogeneous. [Ref. 1: pp. 4-5]

A measure of the general roughness of the surface is given by z_0 , the roughness length. Its value is determined as a function of the mean wind velocity at various elevations above the surface of interest. Combining the roughness length with the elevation and windspeed, both the turbulence intensity and length scale can be determined empirically [Ref. 14: p. 5]. Typical surface roughness lengths for the ocean are $0.001 < z_0 < 0.01$, where z_0 is measured in meters; at a ten meter elevation, this can result in a turbulence intensity range between 13 and 17 percent (see Reference 14 p. 11).

Apparently, the turbulence intensity in the marine surface layer can be significant. However, the effect of such turbulence fluctuations is highly dependent upon the length scales present. For the range of roughness lengths ($0.001 < z_0 < 0.01$) and the elevation ($z = 10$ m) given above, the length scale is approximately 85 meters (see Reference 14 p. 8). This value represents a scale very much larger than a conventional missile, and as such would have little effect on its boundary layer development. Yet, the cascade effect presented above allows for a decrease in the length scale until viscous forces dissipate the energy. Therefore, it is possible that length scales which are initially much larger (for example, approximately 85 meters) than the dimension of a missile would decrease, or "cascade," to scales where they could affect the development of the missile boundary layer.

4. Mach and Reynolds Number Effects

The effect of the Mach number M and the Reynolds number Re on the development of the missile boundary layer and asymmetric vortices is dependent largely on the geometry of the body. Exhaustive research (see References 4, 7, 8, and 6) has been conducted, often with mixed results. The many different combinations of slender noses and afterbodies make comparisons of data very difficult. However, some generalities are possible.

With regard to the Mach number, the magnitude of the side force Y tends to decrease as M is increased. The degree to which the force is reduced, as well as the point at which the reduction becomes significant, is determined by the shape of the body. At one extreme, a blunt-nosed cylinder experiences a rapid drop in Y as the flow approaches transonic velocities. This is caused by the tendency to form a separation bubble at the nose of the blunt cylinder (see Figure 1.1). [Ref. 4: p. 99]

On the other hand, a tangent ogive-nosed cylinder may undergo asymmetric vortex shedding into the supersonic region. Due to the lack of a separation bubble, strong side forces develop which can affect the body significantly. In both the blunt- and ogive-nosed cases, however, the side force Y tends to decrease with increasing Mach number [Ref. 7: p. 5].

The effect of the Reynolds number is best summarized by Ericsson and Reding [Ref. 4: p. 107] ; the vortex-induced side force reaches a maximum at a critical Reynolds number, when conditions are fully subcritical on one side of the body and fully supercritical on the other. A word of caution is necessary; the results for both the Mach and Reynolds number effects are based on several different experiments. Consistencies in data which hold for several body configurations would seem to indicate a valid trend. However, slight changes in test conditions often reverse the previously observed trends. Therefore, the tendency to draw broad conclusions in this area can be severely misleading. Przirembel and Shereda present an enlightening view of this problem in Reference 15.

C. EFFECTS ON VERTICALLY-LAUNCHED SURFACE-TO-AIR MISSILES

The use of vertically-launched surface-to-air missiles (VLSAM) is currently receiving wide acceptance. The advantages presented above demonstrate distinct improvements in reliability and flexibility. However, the flow regime into which a VLSAM is launched is not fully understood. As a result, the aerodynamic effects are difficult to predict. The effect of small-scale turbulence on asymmetric vortices has not yet been examined experimentally. Research into this area is the goal of this thesis.

It is usually desired that experimental research have general application in an area of current interest. For this reason, a generic VLSAM model, similar to current missile designs now in use, was developed by the author for this thesis. This generic design will hereafter be referred to as "the VLSAM" or "the model."

1. Launch and Crosswind Velocities

In order that such research prove to be of current interest, it is necessary to examine the relative velocities of the VLSAM at launch and the crosswind it experiences. Although each type of missile has a different launch velocity vs. time profile, a generic launch profile is used here to demonstrate relative velocities. The generic data presented in Table 1 were provided by Farley (see Reference 16). The data in Table 1 are presented graphically in Figure 1.4.

TABLE 1
GENERIC VLSAM LAUNCH VELOCITY HISTORY

<u>Time (sec)*</u>	<u>Velocity (ft. sec)**</u>
0.0	100
0.2	164
0.5	261
1.0	422

* tail clears launcher exit plane at 0.0 sec

** assumes 10 g missile longitudinal acceleration (generic)

Examination of Figure 1.4 yields a slope of $+322 \text{ ft/sec}^2$. This corresponds to the acceleration in the vertical direction, a_z . Substitution into kinematic equations at time $t = 0.2$ seconds, with a launcher height $z_1 = 30$ ft above the ocean surface, yields a height $z \sim 56$ ft. Thus, while still in the surface layer ($z \sim 50$ m), the VLSAM has a velocity of $V_1 = 164 \text{ ft/sec}$.

The assignment of a crosswind velocity is somewhat more arbitrary. It is dependent on the ambient wind speed, but also on the speed of the launch platform itself. In simplifying the determination of the crosswind speed, a maximum and minimum speed can be selected. With the minimum obviously at zero, the maximum is simply the sum of the mean wind speed and the ship's speed. For a mean windspeed of 20 m sec [Ref. 1: p. 64] and a ship speed of 20 knots, the crosswind speed $V_c \sim 30$ m sec ($= 98 \text{ ft/sec}$).

In a two-dimensional cartesian coordinate system, let $V_c =$ velocity in the x-direction, and $V_1 =$ velocity in the z-direction. Vector addition of the components yields a resultant speed $V_r = 191 \text{ ft/sec}$ at an angle α of 31° from the z-direction (see

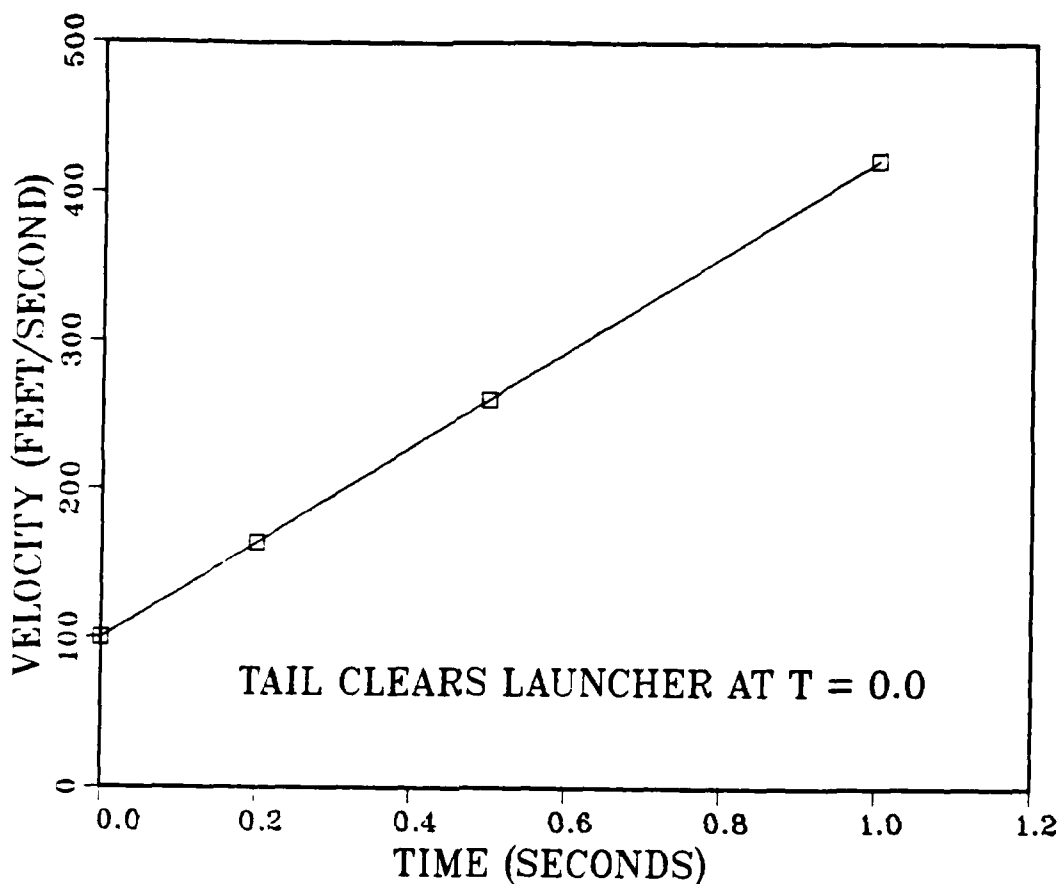


Figure 1.4 Generic VLSAM Launch Velocity versus Time.

Figure 1.5). The direction represents the angle of attack α which the VLSAM experiences while still in the marine surface layer only 0.2 seconds after launch. This places the VLSAM in Regime III, the asymmetric vortex region, almost immediately after clearing the exit plane of the launcher.

2. Other Launch Considerations

There are many factors which affect the aerodynamics of a missile during the launch phase of its flight. Some are inherent to the design of the missile, while the effect of other factors is determined by the ship's orientation at launch. In the former category are plume (or jet) effects of the missile's engine, blast effects of the vented exhaust gases, and activation of the flight control systems. The latter category includes shipboard roll, pitch, and yaw, and ship airwake turbulence.

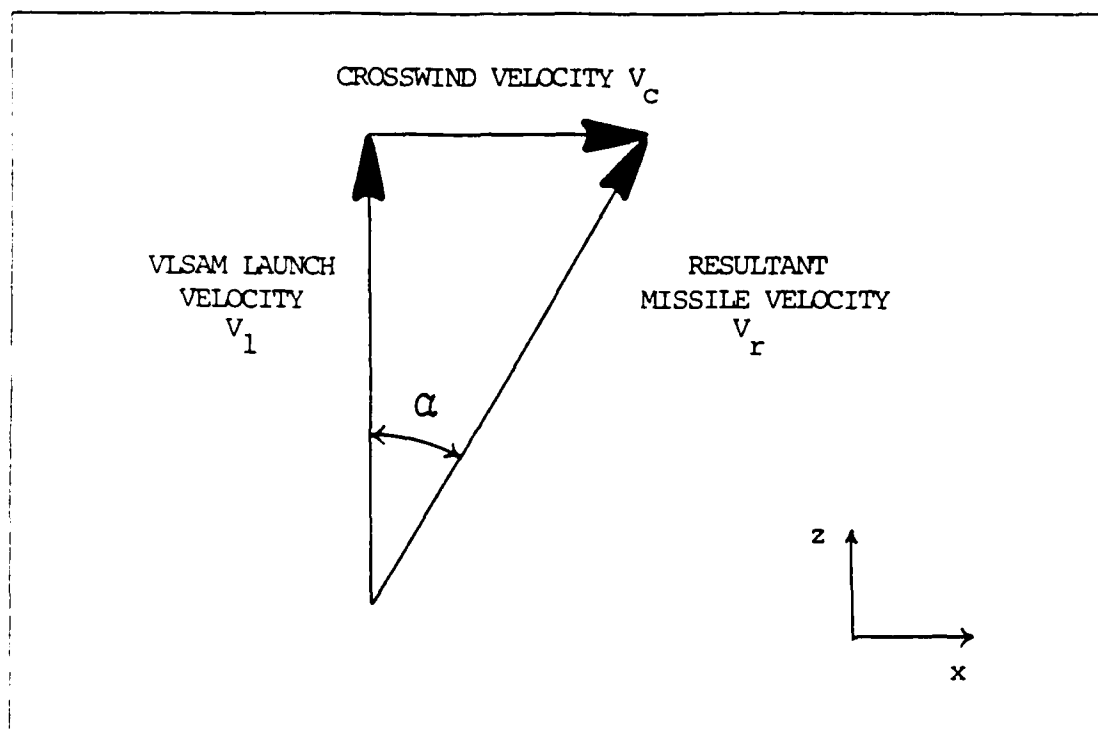


Figure 1.5 Resultant Missile Velocity Vector.

Plume and blast effects can affect the VLSAM in two ways. The first is the direct effect of the propulsion system gases or exhaust gases on the aerodynamic surfaces of the missile. Additionally, the exhaust gases can directly impact the flowfield into which the missile is launched, especially if the gases are vented upward into the vicinity of the accelerating missile.

The manner in which the control systems respond to changes in missile orientation is another factor to be considered. Various systems are employed: some use a simple ballistic flight during the boost phase, while others attempt to maintain the missile's orientation to a reference plane. Matters are further complicated by accounting for the motion of the ship as the missile travels along the guide rail prior to clearing the launcher.

In addition to the turbulence generated in the marine atmospheric boundary layer, turbulence is also present in the airwake generated by flow over the ship's superstructure. The effects of this turbulent ship airwake on the VLSAM are largely unknown. Full understanding of the effects of the airwake on the missile boundary

layer cannot be accomplished, however, without first studying the complex nature of the airwake itself. Research by Healey (see Reference 14) outlines the need for comprehensive experimental work which combines the oscillatory motion of the launching platform with the bluff body turbulence generated by the superstructure.

The above considerations, while not forming a complete description, emphasize the multiple factors which impact upon the flight behavior of a missile during the launch phase. Except for the limited discussion in the preceding paragraphs, these additional effects will not be included in this thesis.

II. EQUIPMENT AND PROCEDURES

A. APPARATUS

The major pieces of equipment utilized in the experimental portion of this thesis consisted of a wind tunnel, a missile model with associated support structures, turbulence-generating grids, and data acquisition hardware software. Information concerning the specifications, construction, and configuration of all equipment used is provided in this section.

1. Wind Tunnel

The wind tunnel utilized for the experimental data was a low-speed, single-return horizontal tunnel installed in Halligan Hall at the Naval Postgraduate School in Monterey, California (see Figure 2.1). It is powered by a 100 horsepower electric motor coupled to a three-blade variable pitch fan via a four-speed Dodge truck transmission. Turning vanes are installed at all four corners, with two small-mesh wire screens installed upstream of the settling chamber. A heavy wire screen is also installed downstream of the test section to prevent damage to the fan blades or turning vanes in the event of model failure during operation. [Ref. 17: pp. 3-1 to 3-7]

The test section of the tunnel measures 45 inches by 32 inches, with corner fillets which house the test section lighting; the cross sectional area is 9.88 square feet. The contraction ratio of settling chamber area to test section area is approximately ten. The walls of the test section diverge slightly to allow for boundary layer growth without a reduction in the freestream pressure along the test section. As the test section is designed to operate at atmospheric pressure, a circumferential breather slot is installed downstream of the test section to replenish air lost through leaks in the tunnel walls. The tunnel was designed to provide velocities up to 290 feet per second in the test section. [Ref. 17: pp. 3-4 to 3-6]

A reflection plane is installed in the floor of the test section, which decreases the vertical dimension to 28 inches. In the center of the reflection plane is a flush-mounted turntable for adjustments in pitch angle. The angle of the turntable is remotely controlled with an electric motor installed beneath the tunnel.

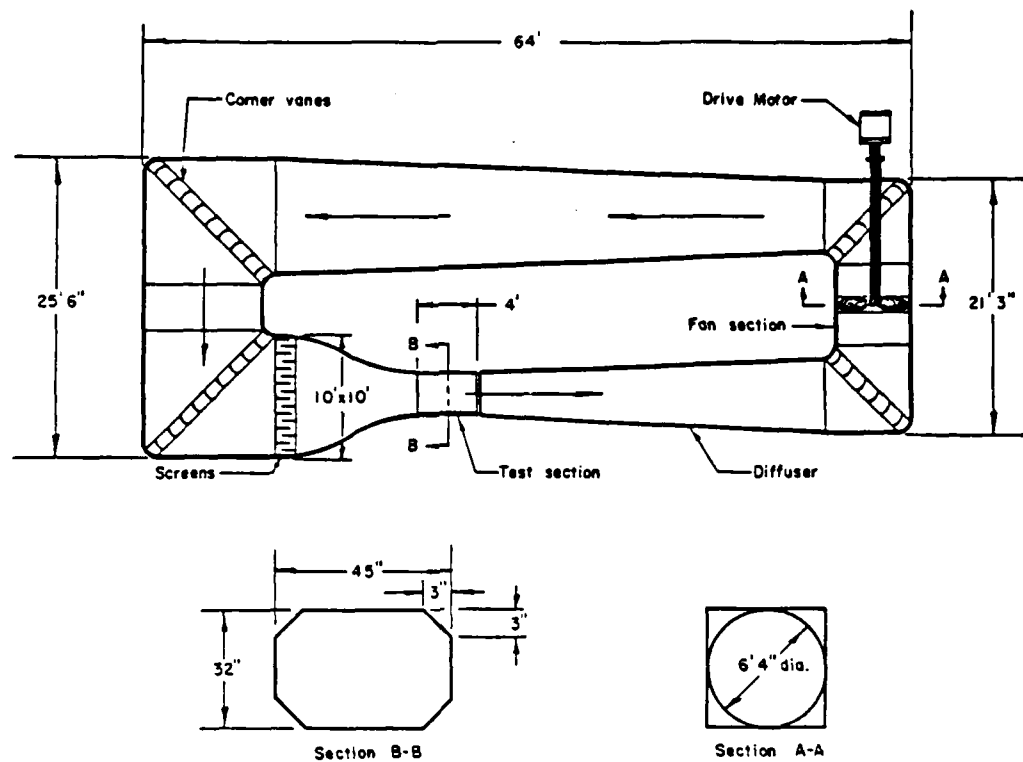


Figure 2.1 Schematic of Wind Tunnel.

2. Turbulence Grids

Four turbulence grids were used in the tunnel. Ideally, such grids would generate isotropic homogeneous turbulence over a range of scales and intensities. All four grids were constructed by the author, and were designed for rapid installation and removal to facilitate maximum data acquisition with minimum tunnel occupation time. Each grid was mounted in a wood frame, which was placed 73 inches ahead of the pitch axis of the model support system (see Figures 2.2 and 2.3). The grids were installed in the tunnel using flush-mounted bolts, which extended through the frame and tunnel walls, and were securely fastened from outside the tunnel. The specifications of the four grids are listed in Table 2.

The wooden turbulence grids used were square-mesh, square-bar biplane grids (see Figure 2.4), while the wire grid was also a square mesh but with round bars. Experience reveals the biplane grid to be superior for the generation of nearly-isotropic

TABLE 2
GRID SPECIFICATIONS

Grid No.	M * in.	d ** in.	M d	Material
1	5.0	1.0	5	wood
2	3.75	0.75	5	wood
3	2.5	0.5	5	wood
4	1.0	0.0625	16	wire

* M = mesh width

** d = bar diameter

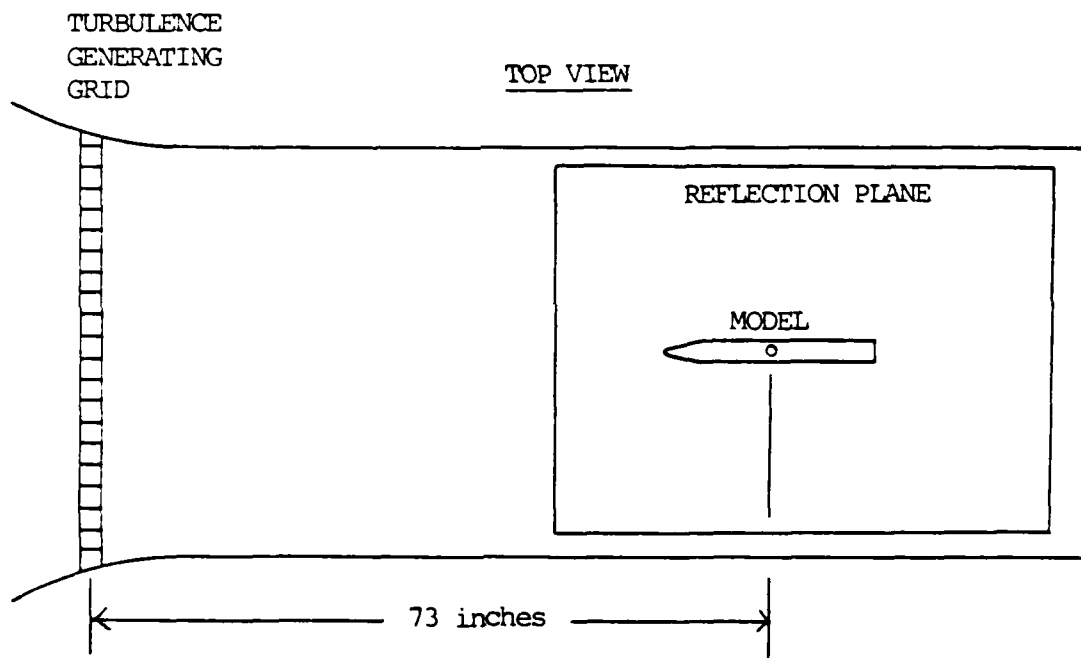


Figure 2.2 Position of Turbulence Grids in Wind Tunnel.

homogeneous turbulence. Both biplane grids with rectangular bars, and monoplane grids, have been shown to produce nonuniform and unsteady flow, possibly caused by the increase in the separated region downstream of each grid intersection [Ref. 11: p. 285]. A drawback of grid-generated turbulence is the fact that it is only

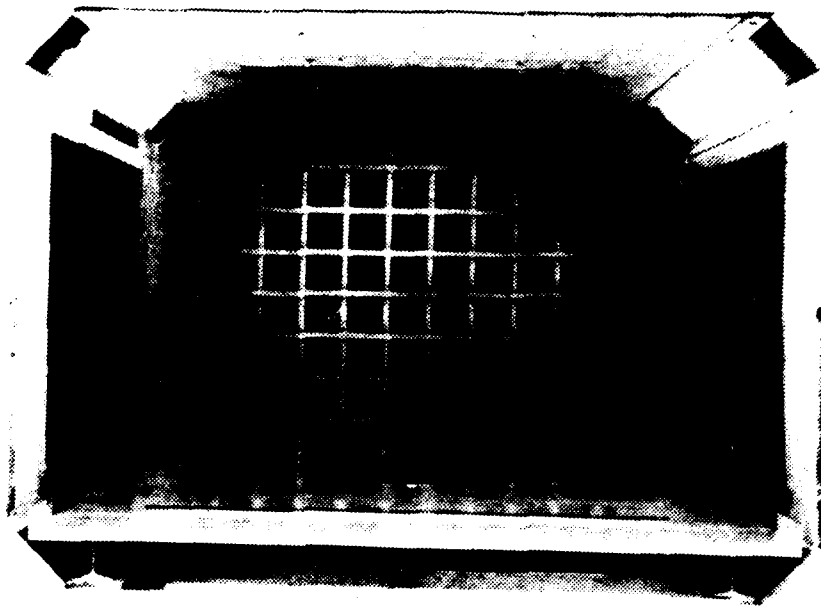


Figure 2.3 Turbulence-Generating Grid Mounted in Wind Tunnel.

nearly - isotropic. Castro [Ref. 18: p. 300] shows the longitudinal rms velocity component to be up to five percent greater than the lateral components. Tunnel blockage with the wooden grids was 20 percent, and 6.25 percent with the wire grid.

3. Missile Model and Support System

The VLSAM model was designed by the author to be representative of current vertically-launched surface-to-air missiles. It is intended to model a cruciform tail-control missile with long dorsal fins (see Figure 2.5); however, all of the "control" surfaces are fixed in position. It was constructed of 6061 and 2024 aluminum alloy by Naval Postgraduate School personnel. It is designed to permit force, moment, and pressure measurements while being operated in a subsonic wind tunnel. The force and moment measurements are accomplished using an internal strain-gage balance mounted on a sting. Pressure measurements are made using pressure taps located just aft of the ogive nose. Due to the dimensions of the model, pressure and force moment measurements cannot be made concurrently. The nose, tail, and dorsal fins are

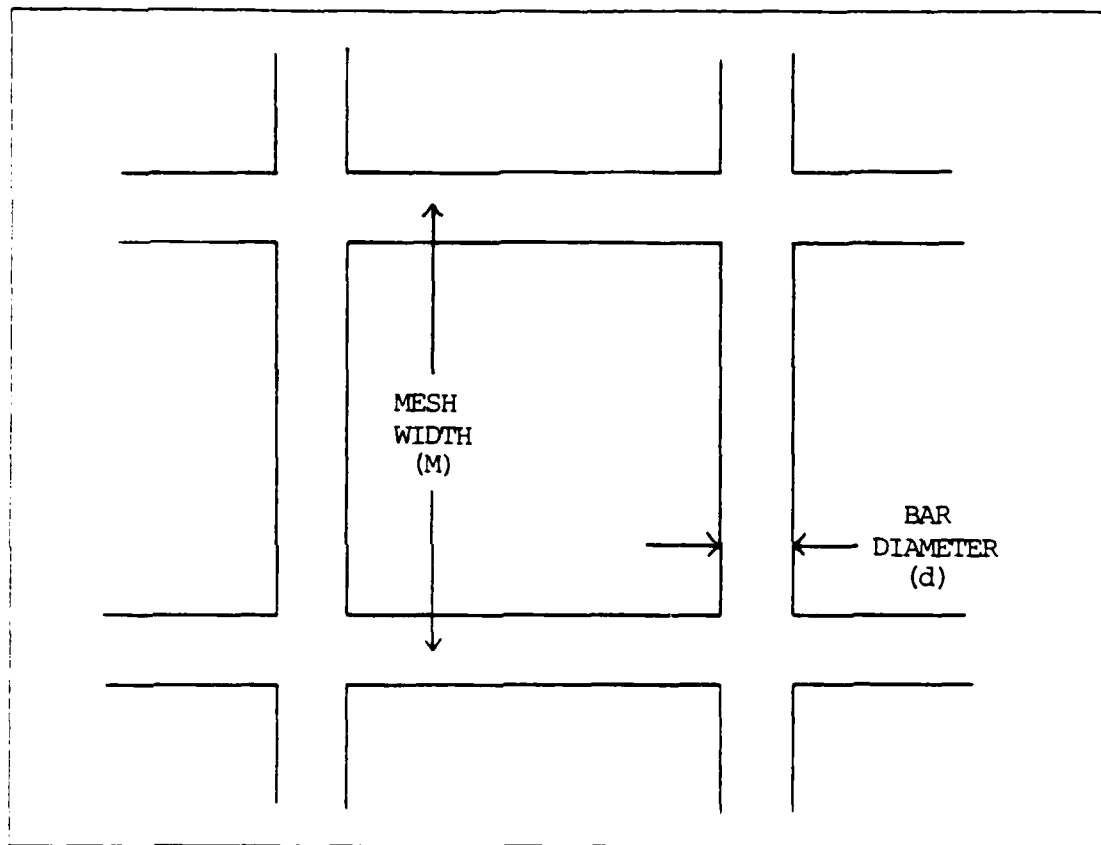


Figure 2.4 Square-Mesh Turbulence-Generating Grid.

removable, both for access to the measurement devices as well as for future configurational changes. The dimensions of the model are summarized below:

- Diameter = 1.75 inches
- Length = 22.85 inches
- Missile length diameter ratio = 13.06
- Ogive nose length = 4.0 inches
- Ogive length diameter ratio = 2.29
- Dorsal span = 3.13 inches
- Tail span = 5.50 inches
- Center of pressure location \sim 13.5 inches aft of nose tip

The support system for the VLSAM missile model was adapted to this wind tunnel by the author; its design and construction allow testing of different models of various configurations. Rigidly mounted to the turntable and supported at the tunnel ceiling, it permits simultaneous variation of the roll and pitch (or yaw) angles.

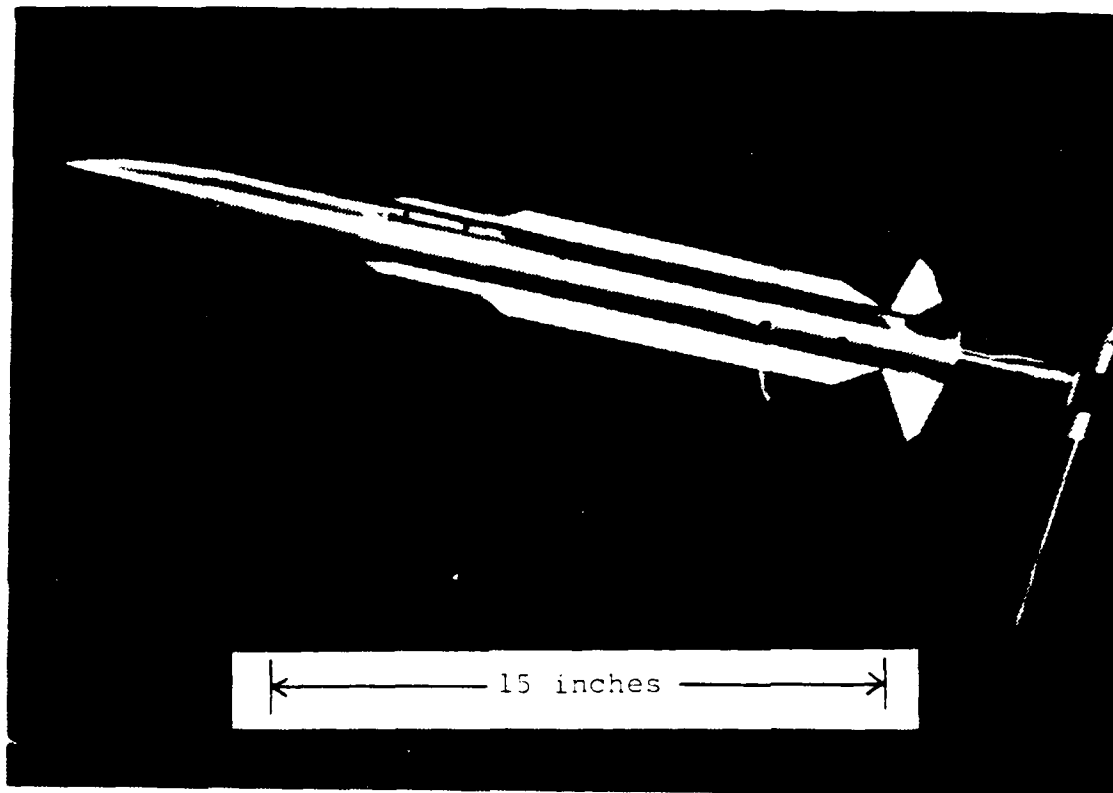


Figure 2.5 VLSAM Missile Model.

4. Hot-Wire Anemometry Equipment

Hot-wire anemometry was utilized to obtain data for longitudinally mapping the turbulence generated in the wind tunnel. Equipment was installed in the tunnel for both the hot-wire calibration and the turbulence mapping. Extensive use was made of existing data acquisition equipment, including computer hardware and software.

a. Calibration Apparatus

The hot-wire calibration system is diagrammed in Figure 2.6. Much of the equipment and computer software used in the calibration was developed for prior wind tunnel research. A Dantec single-sensor wire probe (type 55P11) was installed between two pressure probes, one measuring total pressure and the other measuring static pressure (see Figure 2.7). The hot-wire pressure probe was mounted at the downstream end of the wind tunnel test section. The wire sensor was connected to a DSI Model 10 hot-wire anemometer, while the pressure probes were connected via

transducers to a Paroscientific digital pressure computer. The hot-wire anemometer and the pressure computer were connected to a Hewlett-Packard PC Instruments system, consisting of a relay multiplexer, digital multimeter, digital input output device, and a system power unit. The instrument system interfaced with an IBM Personal Computer AT.

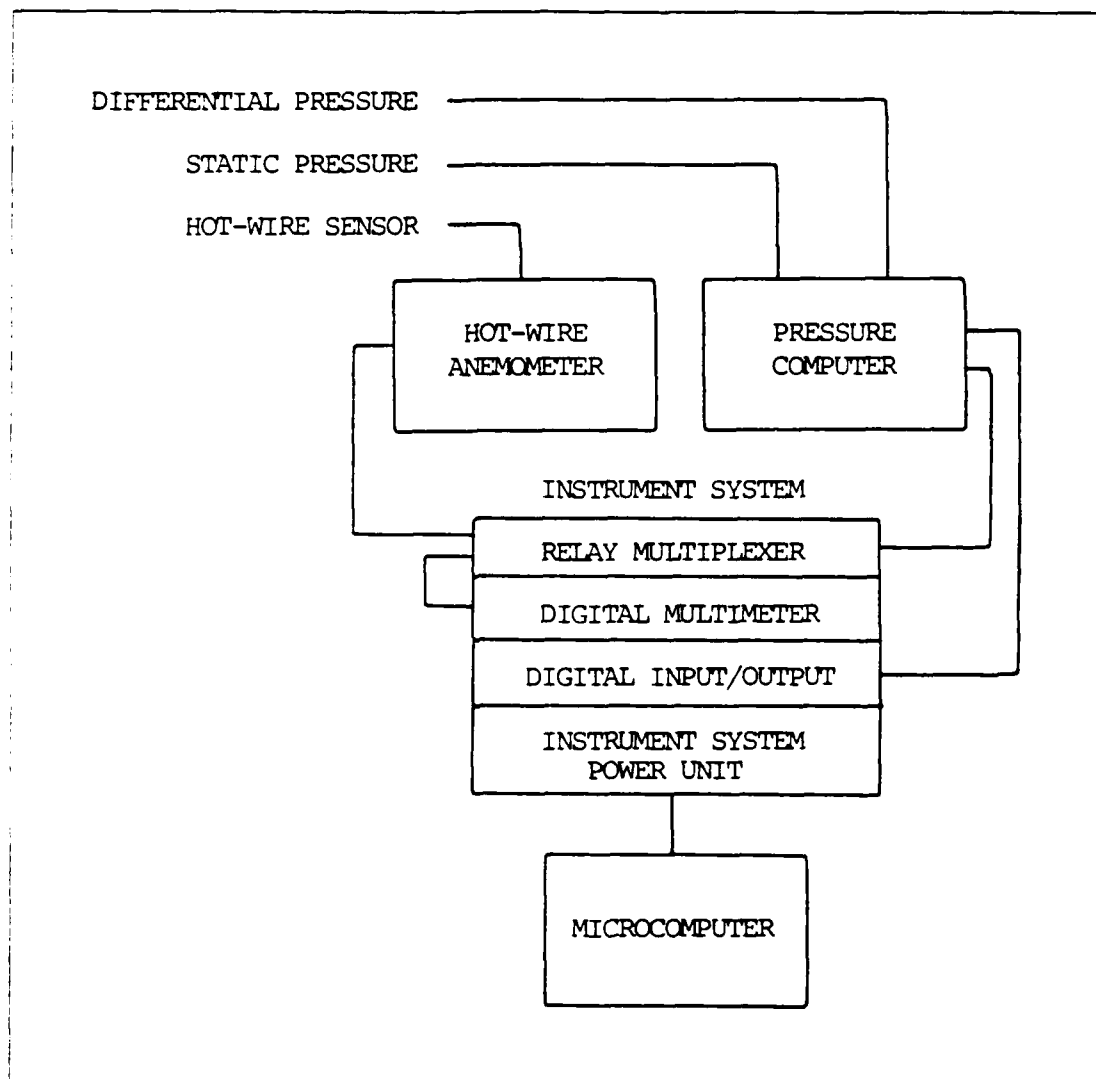


Figure 2.6 Block Diagram of Hot-Wire Calibration Apparatus.

Another major component in the hot-wire calibration system was an interactive computer program designed to facilitate data acquisition (see Reference 19).

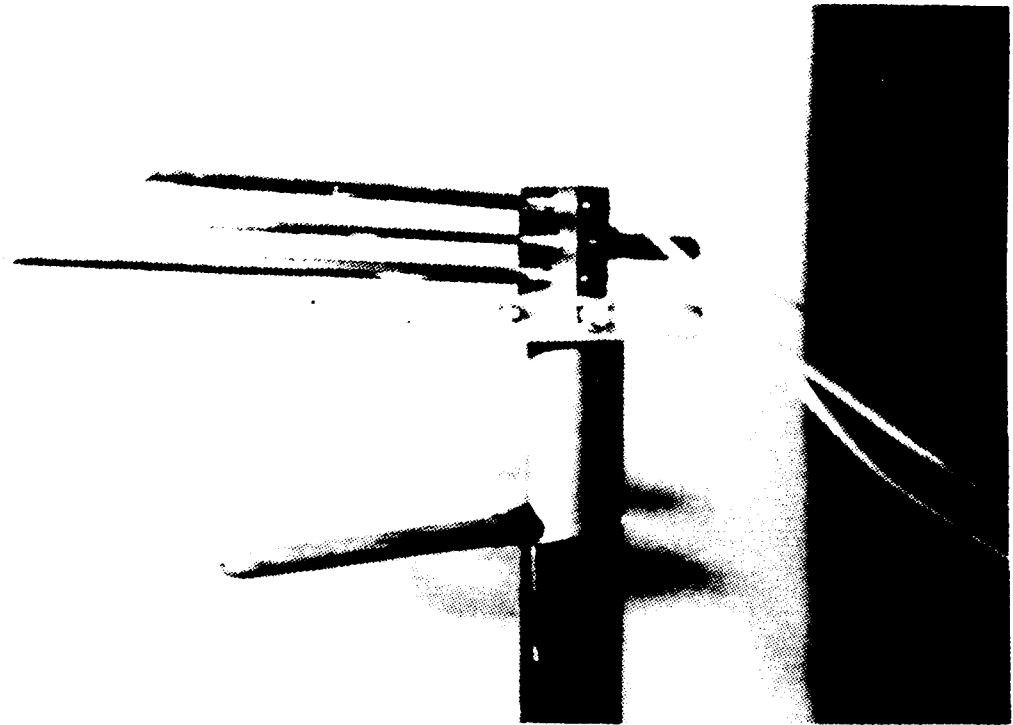


Figure 2.7 Hot-Wire Sensor and Pressure Probes.

Minor modifications to this program were made by the author. The program, CALIB1 (as modified), is contained in Appendix A.

b. Turbulence Mapping Apparatus

The apparatus used for the actual turbulence mapping is diagrammed in Figure 2.8. The hot-wire and anemometer were the same as used in the calibration. Additional equipment included a Tektronix 465M oscilloscope and a Fluke 8050A digital multimeter for acquiring true rms values. The hot-wire probe (see Figures 2.9 and 2.10) was mounted on an aluminum cylinder, approximately centered horizontally and vertically in the wind tunnel. The probe could be positioned between 5 inches and 23 inches upstream of the cylinder, which was rigidly mounted to the floor of the wind tunnel. Additionally, the cylinder itself could be positioned longitudinally in the wind tunnel. Thus, the hot-wire sensor could be positioned in a region extending from the downstream end of the test section to approximately six inches downstream of the turbulence grids.

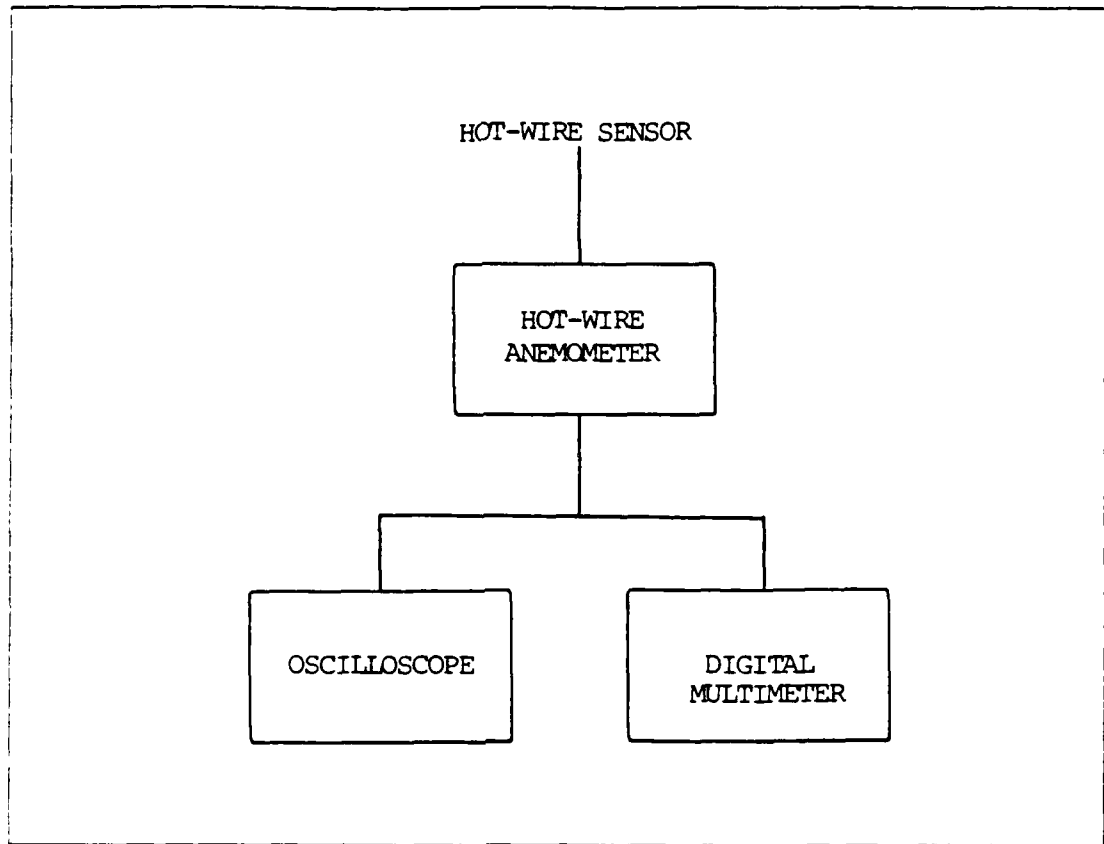


Figure 2.8 Block Diagram of Turbulence Mapping Apparatus.

B. PROCEDURE

1. Hot-Wire Calibration

The purpose of the hot-wire calibration was to generate a curve for correlating voltage fluctuations to velocity fluctuations. The procedure used for hot-wire calibration closely followed that outlined in the TSI anemometer instruction manual and the hot-wire experiment manual [Ref. 19]. The following is a summary of the procedure utilized.

The data acquisition system was configured as shown in Figure 2.6. The hot-wire pressure probe was mounted on a rigid aluminum stand at the downstream end of the test section. A shorting probe was inserted in the probe support and cable resistance was measured and recorded by the anemometer.

The wire sensor probe was then installed in the probe support and probe resistance R_{tot} was measured. The operating resistance R of the probe was then calculated using Equation 2.1,

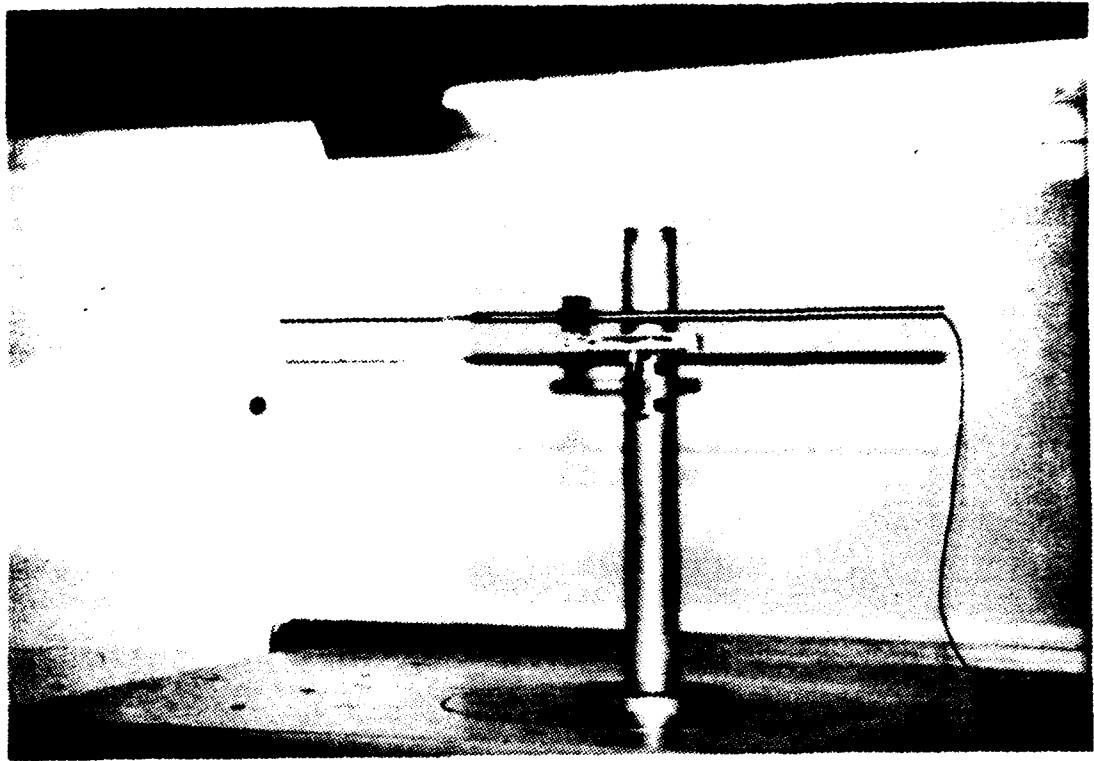


Figure 2.9 Hot-Wire Sensor Mounted For Turbulence Mapping.

$$R = R_{tot} - \alpha_{20} R_{20} (T_s - T_o) \quad (\text{eqn 2.1})$$

where α_{20} and R_{20} are supplied with the wire sensor and T_s is selected by the operator. The calculated value of R was entered into the hot-wire anemometer. The wind tunnel was started and placed in operation at a speed (100 knots) above that expected in the turbulence mapping. The anemometer Wheatstone bridge and cable compensation controls were adjusted, according to the instruction manual, for maximum frequency response. The hot-wire calibration program CALIB1 was then initiated on the microcomputer. The wind tunnel was set to various speeds, using the micromanometer, which extended through the range to be used with turbulence grids in place. The following parameters were recorded for each speed set in the wind tunnel: anemometer output voltage, test section velocity, tunnel temperature, dynamic pressure, static pressure, and air density in the test section. In addition, hot-wire voltage and wind tunnel velocity were stored in a data file for use in generating the

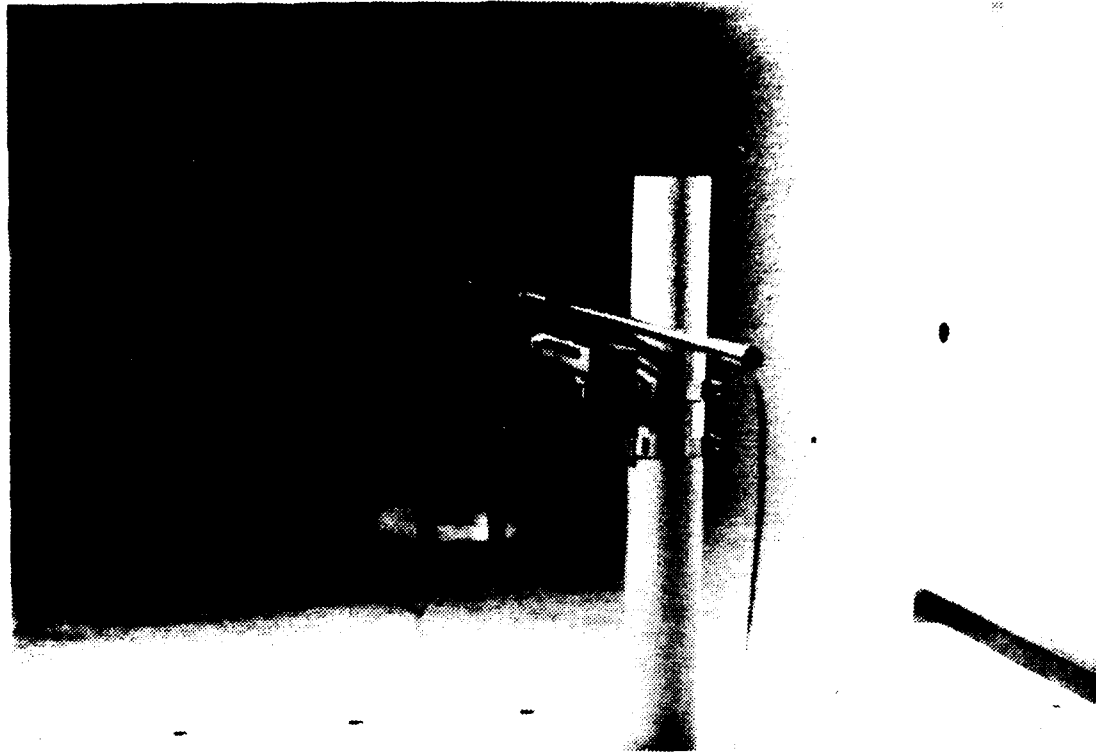


Figure 2.10 Hot-Wire Sensor Downstream of Turbulence Grid.

hot-wire calibration curve. This calibration procedure was conducted both prior to and after obtaining the turbulence mapping data.

2. Turbulence Mapping

The purpose of the turbulence mapping was to determine both the turbulence intensity and length scales as a function of distance downstream of the turbulence-generating grids. It was assumed that the biplanar, square-bar, square-mesh grids generated nearly-isotropic homogeneous turbulence at a large number of mesh widths from the plane of the grid. Therefore, single-wire hot-wire measurements were only made in the center of the tunnel cross-sectional area.

A hot-wire calibration was conducted prior to the commencement of the turbulence mapping. The hot-wire probe support and guide tube were mounted on the aluminum cylinder and positioned in the tunnel. The data acquisition system was then configured as shown in Figure 2.8. The cable resistance previously determined was entered into the hot-wire anemometer. The wire sensor probe was inserted in the

probe support, and the probe operating resistance R was calculated and entered into the anemometer.

The digital multimeter provided an rms value of voltage fluctuations across the wire sensor. As the value displayed changed five times every two seconds, an average based on the values displayed was calculated. Thus, the operator would record the values displayed, then compute the "average" rms voltage fluctuation depending on the number of values recorded. The output voltage was recorded from the display on the hot-wire anemometer, and the signal was monitored on the oscilloscope display.

An initial run was made with no grid in place. The wire sensor was at Position 0 (see Table 3) and 100 rms voltage readings were taken. Subsequent rms voltage averages were made with 50 values. This represented an observation period of approximately 20 seconds.

TABLE 3
HOT-WIRE SENSOR LOCATION

Sensor Position	Distance Downstream From Grid
8	6.88 inches
7	13.88
6	20.88
5	25.13
4	32.13
3	39.13
2	50.63
1	57.63
0	64.63
A	75.13
B	82.13

The following turbulence mapping runs were conducted with the grids in position. Runs were made for each grid with the wire sensor at each of the positions listed in Table 3. Once again, averages were computed for the rms voltage fluctuations, while the output voltage was obtained directly from the anemometer display. During each run, the micromanometer setting and the tunnel temperature

were recorded. The atmospheric pressure was checked and recorded periodically. A hot-wire calibration was conducted following the completion of the turbulence mapping.

III. RESULTS

A. HOT-WIRE ANEMOMETRY

The results of the hot-wire anemometry are separated into two areas; hot-wire calibration and turbulence mapping.

1. Hot-Wire Calibration

Hot-wire calibration was conducted both before and after the turbulence mapping. The results of the two calibrations, presented in Table 4 and Figure 3.1, show a slight divergence between the initial and final runs. Linear equations were generated for each curve in the regions utilized in the turbulence mapping. For a given voltage, the initial and final equations differed by approximately seven percent. The turbulence mapping was evenly distributed over a three day period; therefore, no inference could be made as to which was the "better" curve. Since rms values are presented as a fraction of the local mean velocity, a small error in the calibration has little effect. For this reason, an average of the two equations was used for all further calculations.

In addition, it was determined that the remote thermometer, which was used as an input to the calibration computer program, was unreliable. As a result, a direct reading thermometer was used to correct the velocity values generated by the calibration program. The corrections are reflected in Table 4 and Figure 3.1.

2. Turbulence Mapping

The turbulence mapping yielded a large amount of data which was used in the determination of turbulence intensities and length scales. As discussed in Chapter II, the rms voltage resulting from velocity fluctuations was averaged from a large number of readings (at least 50 for each run), each reading itself being a mean of values performed internal to the true rms multimeter. A statistical analysis of the rms readings at Position 0 yielded a mean standard deviation of less than 6 percent of the average rms value for each grid. The hot-wire anemometry system electrical noise was less than 0.5 millivolts; as a result, its effect was negligible. The results of the turbulence mapping are presented in Tables 5, 6, 7 and 8, as well as in Figure 3.2.

TABLE 4
HOT-WIRE CALIBRATION RESULTS

INITIAL		FINAL	
Wire Voltage (volts)	Velocity (ft sec)	Wire Voltage (volts)	Velocity (ft sec)
0.968	0.00	1.394	65.82
1.278	46.64	1.426	73.59
1.337	61.70	1.447	80.62
1.384	65.95	1.470	87.14
1.414	73.75	1.502	98.81
1.433	80.79	1.527	106.71
1.452	85.80	1.545	116.44
1.483	100.44	1.565	126.59
1.510	108.94	1.577	132.98
1.528	116.14	1.592	142.97
1.542	125.21	1.604	149.61
1.560	134.69	1.613	156.93
1.570	141.68	1.620	163.05
1.581	147.43	1.629	170.71
1.593	156.52	1.634	175.62
1.601	162.63		
1.607	169.34		
1.612	175.24		
1.618	181.70		
1.624	190.16		

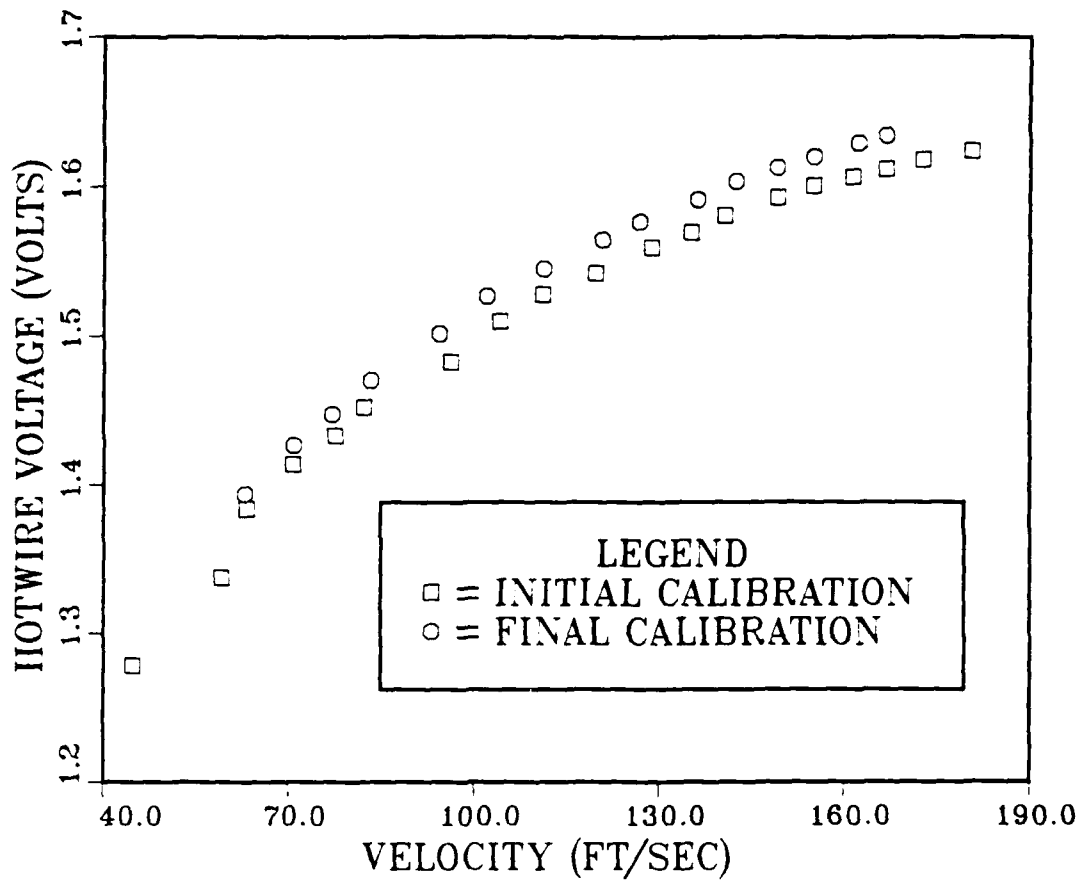


Figure 3.1 Hot-Wire Calibration Results.

The turbulence of the tunnel, with no grid in place, was calculated with a mean voltage of 1.582 volts and an rms voltage of 0.86 millivolts; the turbulence intensity of the tunnel was 0.23 percent. Each of the runs with the wood grids (Grids #1, #2, and #3) was conducted with a dynamic pressure $q = 10.00 \text{ cm H}_2\text{O}$. This resulted in a fairly consistent mean voltage. (The dynamic pressure was used only to ensure similar wind tunnel velocities for each run; with the grids in place the actual value of the dynamic pressure, determined from the static rings, was in error due to the grid frame disturbance.) The wire grid (Grid #4) had to be run at a significantly lower dynamic pressure, $q = 5.45 \text{ cm H}_2\text{O}$, to obtain mean voltages which were similar to those obtained with the wood grids. The difference was caused by the much smaller pressure loss across the wire grid (blockage = 6.25%) as compared to the wood grids (blockage = 20%).

TABLE 5
TURBULENCE DATA FOR GRID #1

Sensor Position	X (inches)	Mean Voltage (volts)	RMS Voltage (millivolts)
8	6.88	1.511	60.58
7	13.88	1.495	45.51
6	20.88	1.497	33.01
5	25.13	1.498	27.86
4	32.13	1.497	23.09
3	39.13	1.495	19.67
2	50.63	1.510	15.41
1	57.63	1.513	13.72
0	64.63	1.516	12.82
A	75.13	1.536	11.56
B	82.13	1.539	10.70

TABLE 6
TURBULENCE DATA FOR GRID #2

Sensor Position	X (inches)	Mean Voltage (volts)	RMS Voltage (millivolts)
8	6.88	1.438	64.84
7	13.88	1.469	39.66
6	20.88	1.490	27.31
5	25.13	1.490	21.85
4	32.13	1.498	17.99
3	39.13	1.508	15.56
2	50.63	1.525	12.77
1	57.63	1.518	11.44
0	64.63	1.512	10.45
A	75.13	1.532	9.71
B	82.13	1.530	9.07

TABLE 7
TURBULENCE DATA FOR GRID #3

Sensor Position	X (inches)	Mean Voltage (volts)	RMS Voltage (millivolts)
8	6.88	1.455	44.81
7	13.88	1.489	25.50
6	20.88	1.497	17.97
5	25.13	1.512	14.55
4	32.13	1.515	11.79
3	39.13	1.510	10.28
2	50.63	1.518	8.44
1	57.63	1.523	7.83
0	64.63	1.528	7.30
A	75.13	1.537	6.62
B	82.13	1.542	6.31

TABLE 8
TURBULENCE DATA FOR GRID #4

Sensor Position	X (inches)	Mean Voltage (volts)	RMS Voltage (millivolts)
8	6.88	1.480	5.99
7	13.88	1.490	5.69
6	20.88	1.491	4.30
5	25.13	1.504	3.62
4	32.13	1.504	3.06
3	39.13	1.505	2.65
2	50.63	1.523	2.11
1	57.63	1.524	1.94
0	64.63	1.521	1.81
A	75.13	1.529	1.65
B	82.13	1.527	1.60

a. Turbulence Intensity

The equation of the average calibration curve was used to determine the mean velocity of the wind tunnel at each position and corresponding mean voltage listed in Tables 5 - 8. Additionally, the slope of the curve was calculated to yield the ratio of the change in velocity to the change in voltage. This ratio was calculated for each position and rms voltage in the above tables.

The hot-wire apparatus measured the resultant of the longitudinal and lateral components of the turbulence. For grid-generated turbulence, the ratio of the longitudinal rms intensity to that of the lateral component is approximately 1.05 [Ref. 18: p. 300]. This difference was accounted for in calculating the longitudinal turbulence intensity $u' U$ from the measured velocity fluctuation P' and the mean velocity U . Thus, the actual longitudinal turbulence intensity was obtained from the measured, two-component velocity fluctuation using Equation 3.1

$$u' U = 0.724 (P' U) \quad (\text{eqn 3.1})$$

The calculated values for turbulence intensity are shown in Table 9 and Figure 3.2 (see also Appendix B).

Inspection of Figure 3.2 shows somewhat erratic behavior close to the grids. Most notable is the magnitude of the turbulence intensity immediately downstream of Grids #1 and #2. The smaller-mesh Grid #2 generated higher T_u than the larger-mesh Grid #1. This discrepancy was most probably caused by the lateral position of the sensor with respect to the grids. For Grid #1, the sensor was positioned downstream of an "open" region between the square bars; for Grid #2, the sensor was downstream of a grid intersection. The data from Table 5 show a relatively high mean voltage for Grid #1 (Position 8), while Table 6 shows a relatively high rms voltage for Grid #2 at the same position.

The above inconsistencies occurred within two mesh widths (2M) for both grids. Previous experimental data show a minimum of 6M is required for the flow to achieve reasonable homogeneity [Ref. 18: p. 300]. Thus, for all the grids evaluated, the data should not be considered homogeneous for the first 30 inches; this corresponds to Positions 8 through 4. The relative turbulence intensity of the four grids at Position 0, which corresponds to a position on the nose of the missile model, is shown in Figure 3.3.

TABLE 9
GRID-GENERATED TURBULENCE INTENSITIES

Sensor Position	Turbulence Intensity (percent)			
	Grid #1	Grid #2	Grid #3	Grid #4
8	17.42	20.66	13.93	1.80
7	13.37	12.08	7.55	1.68
6	9.67	8.08	5.26	1.27
5	8.15	6.46	4.18	1.05
4	6.76	5.26	3.37	0.89
3	5.78	4.49	2.96	0.77
2	4.44	3.60	2.40	0.60
1	3.93	3.25	2.22	0.55
0	3.66	3.00	2.05	0.51
A	3.22	2.72	1.84	0.46
B	2.97	2.54	1.74	0.45

A final observation involves the "character" of the generated turbulence. For all data runs, with one exception, the oscilloscope displayed a "uniformly random" pattern of high-frequency turbulence. In other words, the voltage fluctuations appeared to be continuous and relatively uniform across the oscilloscope. However, for Grid #1, with the sensor close to the grid (Position 8), the voltage fluctuations were interspersed with periods of almost no disturbance. The appearance was that of high-frequency turbulent fluctuations punctuated by bursts of laminar flow, indicating "smooth" airflow between turbulent vortices. The disparity in turbulence between Grid #1 and Grid #2 is further explained by the appearance of these laminar bursts; as laminar flow increases, the rms voltage fluctuations decrease, which lowers the turbulence intensity.

b. Turbulence Length Scale

The turbulence length scales were calculated using the turbulence intensities at the recorded positions. Meier [Ref. 20: p. 7] described a method for correlating the decay of the turbulence intensity with the distance downstream of a generating grid. Furthermore, Hancock [Ref. 11: p. 285] and Castro [Ref. 18: p. 300] link the dissipation length scale L_e with the decay of turbulence intensity.

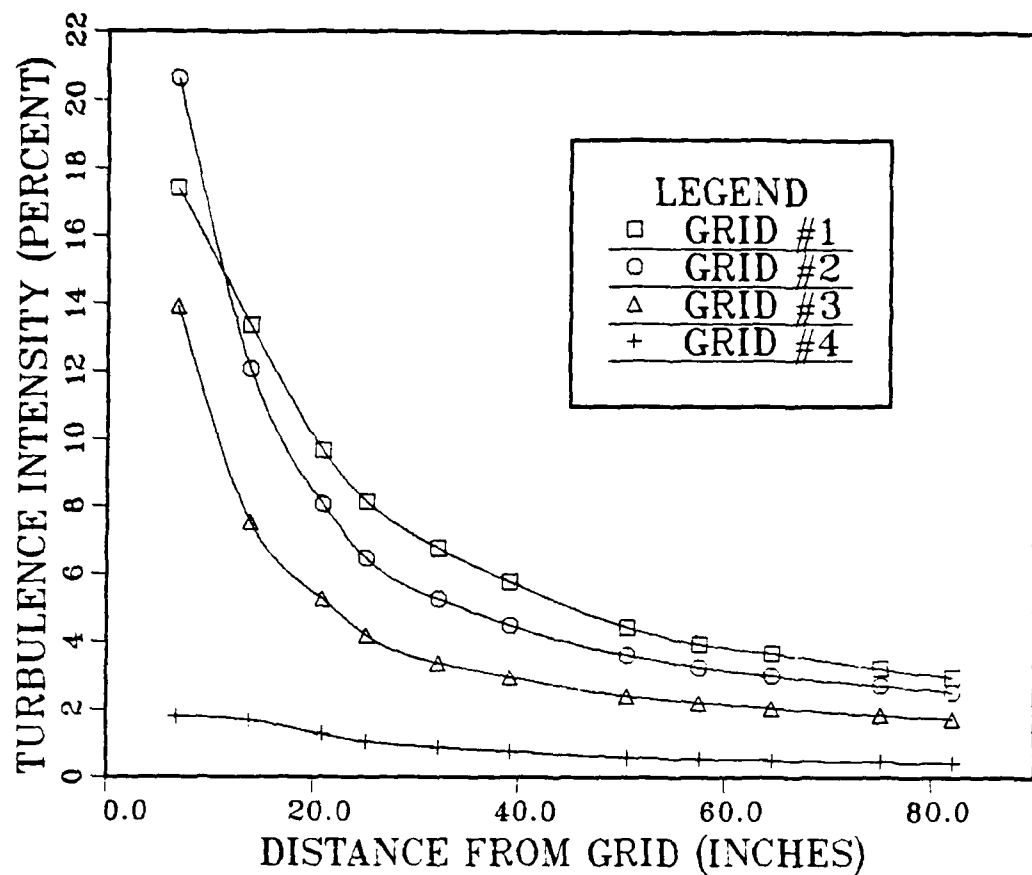


Figure 3.2 Grid-Generated Turbulence Intensity Curves.

Linear approximation of the curves $(T_u^2)^{-0.8}$ versus downstream distance "x" yields lines of the form of Equation 3.2.

$$(T_u^2)^{-0.8} = A(x \cdot M - B) \quad (\text{eqn 3.2})$$

where A and B are constants to be determined for each grid [Ref. 11: p. 285]. The above linear approximations are combined with Equation 3.3

$$U \left(\frac{du^2}{dx} \right) = - (u')^{1.5} L_e \quad (\text{eqn 3.3})$$

and solved simultaneously [Ref. 11: p. 285]. The solution of these equations yields Equation 3.4.

$$L_e \cdot M = 0.8 (A^{-0.625})(x \cdot M - B)^{0.375} \quad (\text{eqn 3.4})$$

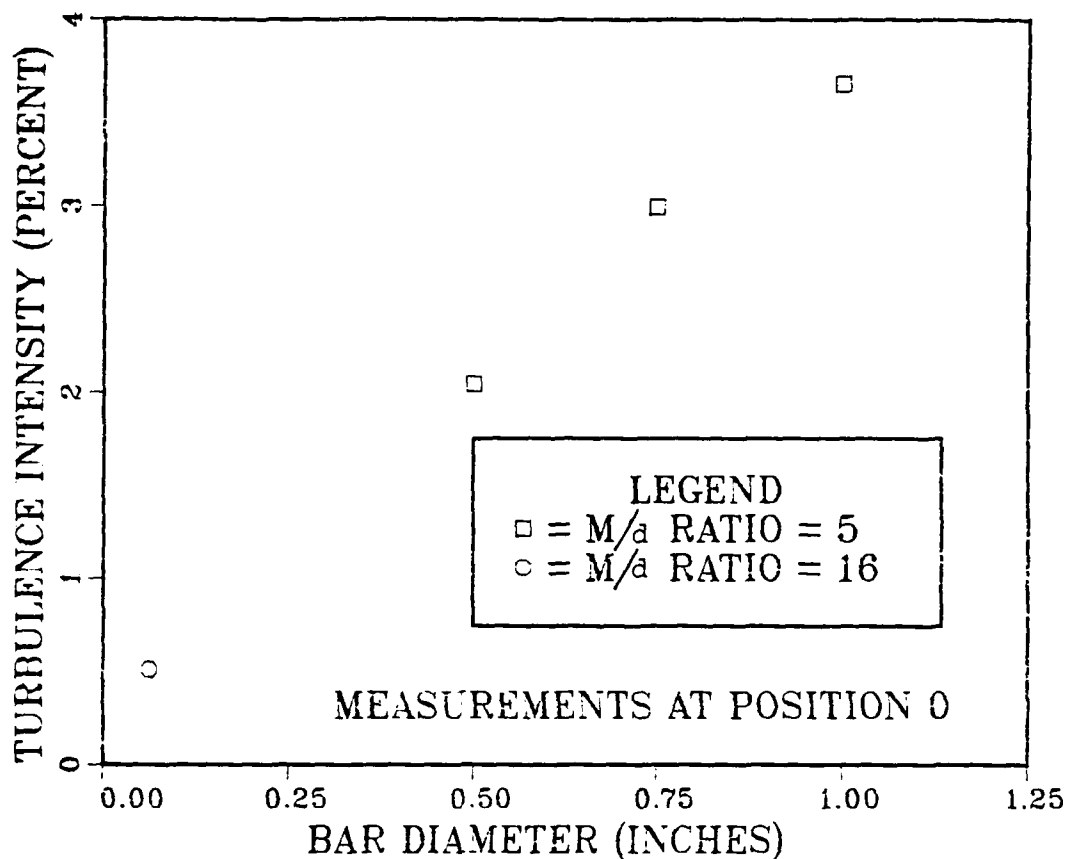


Figure 3.3 Turbulence Intensity at Position 0 in Wind Tunnel.

relating the length scale and the longitudinal distance. Thus, the constants A and B were obtained for each grid. Substitution into Equation 3.4 gave the length scale L_e , presented in Table 10 and Figure 3.4 (see also Appendix B).

These results show a gradual increase in the length scale with increasing distance from the grid. As presented in Chapter I, this increase is due primarily to the cascade effect. As the turbulent eddies "cascade" to smaller length scales, they decay more rapidly due to viscosity. In turn, the "average" length scale, in effect, becomes larger with increasing distance from the grid. Thus, the increase in length scales shown in Table 10 also indicates the presence of smaller, more rapidly dissipated length scales. It is the smaller length scales, on the order of the boundary layer thickness, which affect the development of the boundary layer. The relative turbulence length scale of the four grids at Position 0, which corresponds to a position on the nose of the missile model, is shown in Figure 3.5.

TABLE 10
GRID-GENERATED LENGTH SCALES

Sensor Position	Length Scale (inches)			
	Grid #1	Grid #2	Grid #3	Grid #4
8	1.02	0.84	0.55	0.14
7	1.16	0.97	0.64	0.16
6	1.27	1.06	0.72	0.18
5	1.34	1.12	0.76	0.19
4	1.43	1.20	0.82	0.21
3	1.51	1.27	0.87	0.22
2	1.64	1.38	0.95	0.24
1	1.70	1.44	0.99	0.25
0	1.77	1.50	1.03	0.26
A	1.86	1.57	1.09	0.27
B	1.91	1.62	1.12	0.28

An additional observation from Table 10 and Figure 3.4 is the comparison between the bar diameter of the grid and the length scale at Position 8. At that point, all of the square-bar grids (Grids #1, #2, and #3) yield a length scale which is only ten percent greater than the respective bar diameter. These three grids all have a M/d ratio of five. On the other hand, the wire grid (Grid #4) is a round-bar grid with a M/d ratio of sixteen; at Position 8, its length scale is more than twice the bar diameter.

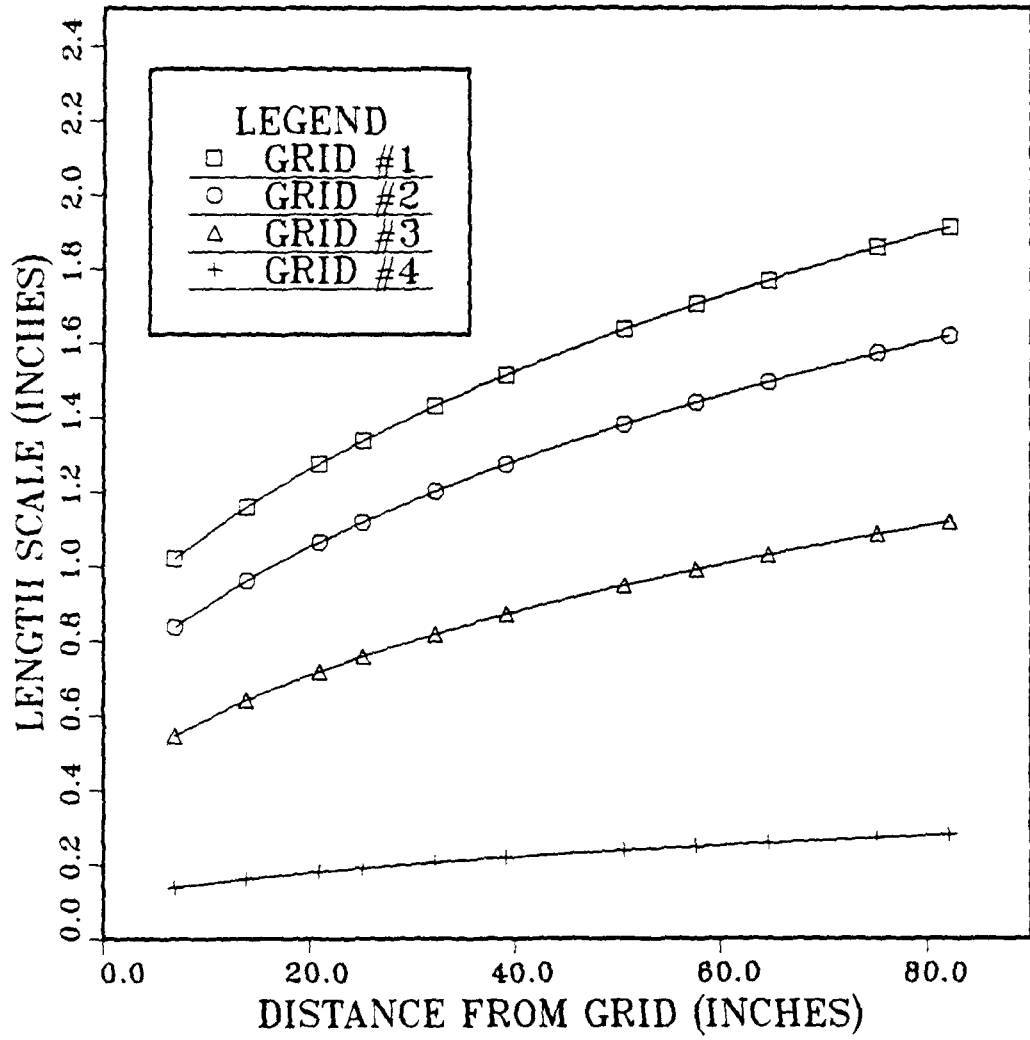


Figure 3.4 Grid-Generated Length Scale Curves.

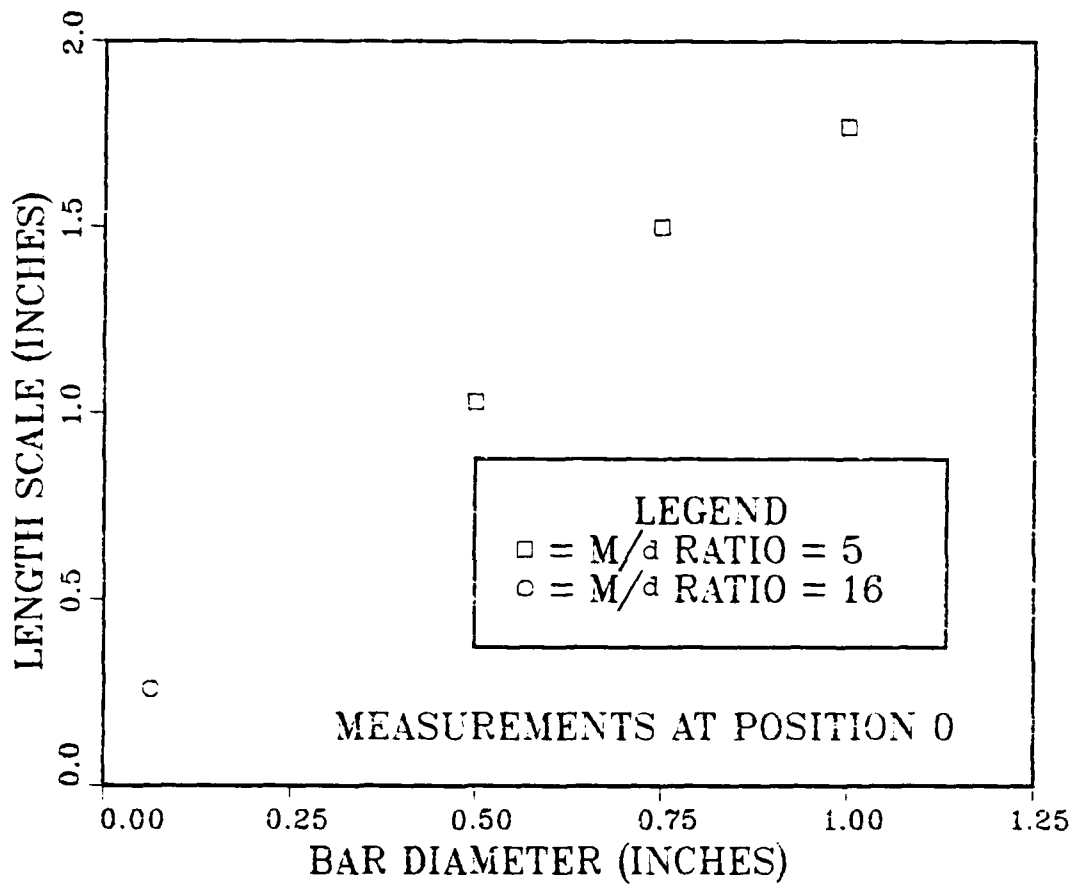


Figure 3.5 Turbulence Length Scale at Position 0 in Wind Tunnel.

IV. CONCLUSIONS AND RECOMMENDATIONS

This experimental study has established a basis for further research on a vertically-launched surface-to-air missile in a turbulent flowfield at high angles of attack. The development of a generic VLSAM model, as well as the data collected and analyzed during the wind tunnel turbulence mapping, serve as a foundation for the continuation of this experimental work at the Naval Postgraduate School.

The turbulence mapping yielded several important points relevant to the effect of turbulence on the development of asymmetric vortices and the missile boundary layer. Of primary importance was the determination of the length scales for each of the grids. Calculations showed that the length scale increased with increasing distance from the grid. This was caused by the dissipation of the smaller length scales which result from the cascade effect. As the smaller eddies dissipate due to viscosity, the proportion of larger eddies becomes greater, effectively increasing the "average" length scale. However, it is not the increase which is of interest, but rather the difference in the magnitude of the scales generated by the various grids. Increasing the bar diameter d resulted in increased length scale L_e . As the parameter of interest is the relation between the length scale and boundary layer thickness, such a variation would appear necessary to allow testing of the model under different flow conditions.

The turbulence intensity was found to increase with increasing bar diameter. The intent is to model turbulence intensities which might realistically be encountered during the launch of a VLSAM. As with the length scales, variation of the turbulence intensities, between the extremes, is considered necessary for validating experimental results. In both instances (L_e and T_u), however, it must be remembered that a suitable distance must be maintained from the grid to allow the flow to develop reasonable homogeneity; data collected near the generating grid may be affected by vortices trailing off of the grid bars.

Although additional research and experimental studies of the VLSAM have already begun, recommendations for additional research are included. As noted above, the VLSAM model has been designed for force, moment and pressure measurements. Therefore, a full set of experimental studies should be conducted, to include force moment data and pressure measurements at all roll angles and angles of attack.

These experiments should be further supported by surface and flowfield flow visualization and hot-wire measurements of the vortex flowfield. This would allow correlation of the turbulence intensities and length scales with the boundary layer development, asymmetric vortex formation and the resultant side forces. Alterations and modifications should be made to the ogive nose and dorsal tail fins to examine the effect of such changes on the development. Finally, after obtaining extensive experimental data, the results should be compared with predictions or models of turbulent flowfields over slender bodies of revolution at high angles of attack.

APPENDIX A

HOT-WIRE CALIBRATION COMPUTER PROGRAM

The computer program CALIBI was utilized in the format shown below. The program shell, which precedes the main program and configures the instruments, is not listed.

Adjustments to the original program (see Reference 19) were intended to eliminate options not required for the hot-wire calibration, as well as to improve the accuracy of the data obtained. The call to the subroutines for reading and selecting angle of attack (Lines 4940-5450) was deleted. Additionally, the arrays for the hot-wire voltage and pressure differential were enlarged to accommodate a greater number of data points for each reading.

After obtaining the calibration curves, however, it was discovered that several additional corrections were necessary. These included scaling the velocities obtained to reflect the use of a direct-reading thermometer. Additionally, Line 4860 adjusts the dynamic pressure, obtained from the pressure probes mounted adjacent to the hot-wire sensor (see Figure 2.7), using the correction factor (0.93) for the tunnel static rings. This adjustment was determined to be incorrect, and the data obtained from the program were corrected accordingly.

```

1000 ' PROGRAM "CALIB1"
1010 OPTION BASE 1
1020 WANTAOA = 0
1030 '
1040 '
1050 ' SET HP BOXES TO INITIAL SETTINGS FOR DATA ACQUISITION
1060 '
1070 '
1080 FILES = "HOTWIRE.HPC"
1090 CALL INITIALIZE.SYSTEM(FILES)
1100 CALL ENABLE.SYSTEM
1110 CALL SET.FUNCTION(DMM.01,DCVOLTS)
1120 CALL SET.RANGE(DMM.01,AUTOM)
1130 CALL SET.SPEED(DMM.01,R2.5)
1140 CALL ENABLE.INT.TRIGGER(DMM.01)
1141 CALL SET.NUM.BITS(DIG.IN.01,R16)
1142 LEVEL = 5
1143 CALL SET.THRESHOLD(DIG.IN.01,LEVEL)
1150 '
1160 '
1170 ' PRINT FIRST SCREEN
1180 '
1190 '
1200 BEEP
1210 CLS
1220 COLOR 4: LOCATE 5,14: PRINT "*****"
*****"
1230 LOCATE 9,14: PRINT "*****" *****"
1240 COLOR 1: LOCATE 9,37: PRINT "PART 1": LOCATE 10,33: COLOR 4: PRINT "*****"
*****"
1250 LOCATE 6,14: PRINT "*": LOCATE 7,14: PRINT "*": LOCATE 8,14: PRINT "*"
1260 LOCATE 6,65: PRINT "*": LOCATE 7,65: PRINT "*": LOCATE 8,65: PRINT "*"
1270 COLOR 1: LOCATE 7,18: PRINT "WELCOME TO THE HOT WIRE FLOW MEASUREMENT LAB"
1280 LOCATE 12,27: PRINT "THESIS BY LT GREG DOREMUS"
1290 LOCATE 15,20: PRINT "THIS PROGRAM IS USED IN CALIBRATING THE "
1300 LOCATE 17,13: PRINT "HOT WIRE SYSTEM FOR WIND TUNNEL AIR FLOW MEASUREMENTS"

1310 COLOR 4: LOCATE 21,24
1320 INPUT "ENTER 1 TO CONTINUE, 2 TO ABORT";ANS1
1330 IF ANS1 <> 2 GOTO 1340 ELSE 5950
1340 CLS: LOCATE 10,36: COLOR 20: PRINT "WAIT...": COLOR 1
1390 '
1400 '
1410 ' PRINT SECOND SCREEN
1420 '
1430 '
1440 CLS: LOCATE 6,10: PRINT "TO START THIS EXPERIMENT YOU MUST FIRST SET UP THE
HOT WIRE"
1450 LOCATE 8,12: PRINT "SYSTEM. THE HOT WIRE LABORATORY MANUAL WILL EXPLAIN THI
S"
1460 LOCATE 10,6: PRINT "PROCEDURE IN DETAIL. ONCE THE SYSTEM SET UP IS TO YOUR
SATISFACTION"
1470 LOCATE 12,10: PRINT "YOU MUST MANUALLY START THE WIND TUNNEL AND SET THE SL
OWEST"
1480 LOCATE 14,16: PRINT "TUNNEL VELOCITY YOU WILL USE IN YOUR EXPERIMENT."
1490 COLOR 4: LOCATE 20,24: PRINT "ENTER 1 TO CONTINUE, 2 TO ABORT"
1500 LOCATE 21,28: INPUT "OR 3 TO GO BACK ONE PAGE";ANS2
1510 COLOR 1: ON ANS2 GOTO 1560,5950,1210
1520 '
1530 ' PRINT THIRD SCREEN - START WIND TUNNEL

```

```

1540 '
1550 '
1560 CLS: LOCATE 10,22: PRINT "IF HOTWIRE SYSTEM IS SET UP PROPERLY"
1570 COLOR 4: LOCATE 12,29: PRINT "START WIND TUNNEL NOW"
1580 LOCATE 20,24: PRINT "ENTER 1 TO CONTINUE, 2 TO ABORT"
1590 LOCATE 21,28: INPUT "OR 3 TO GO BACK ONE PAGE"; ANS3
1600 COLOR 1: ON ANS3 GOTO 1610,5950,1440
1540 '
1550 '
1560 CLS: LOCATE 10,22: PRINT "IF HOTWIRE SYSTEM IS SET UP PROPERLY"
1570 COLOR 4: LOCATE 12,29: PRINT "START WIND TUNNEL NOW"
1580 LOCATE 20,24: PRINT "ENTER 1 TO CONTINUE, 2 TO ABORT"
1590 LOCATE 21,28: INPUT "OR 3 TO GO BACK ONE PAGE"; ANS3
1600 COLOR 1: ON ANS3 GOTO 1610,5950,1440
1610 '
1620 '
1630 ' PRINT FOURTH SCREEN
1640 '
1650 '
1660 CLS: LOCATE 8,13: PRINT "A SERIES OF WIND VELOCITY MEASUREMENTS IS TO BE TA
KEN"
1670 LOCATE 10,12: PRINT "AT WIND SPEEDS VARYING FROM THE SLOWEST TUNNEL VELOCIT
Y"
1680 LOCATE 12,11: PRINT "TO BE USED IN YOUR EXPERIMENT UP TO THE HIGHEST VELOCIT
Y."
1690 LOCATE 14,15: PRINT "A MINIMUM OF 10 READINGS SHOULD BE TAKEN TO CREATE"
1700 LOCATE 16,29: PRINT "THE CALIBRATION CURVE."
1710 COLOR 4: LOCATE 20,24: PRINT "ENTER 1 TO CONTINUE, 2 TO ABORT"
1720 LOCATE 21,28: INPUT "OR 3 TO GO BACK ONE PAGE";ANS4
1730 COLOR 1: ON ANS4 GOTO 1790,5950,1560
1740 '
1750 '
1760 ' ENTER DATA POINTS FOR CALIBRATION CURVE
1770 '
1780 '
1790 CLS: LOCATE 12,12: PRINT "ENTER THE                                YOU WILL TAKE TO
CREATE"
1800 COLOR 4: LOCATE 12,22: PRINT "NUMBER OF DATA POINTS": COLOR 1
1810 LOCATE 14,19: INPUT "THE CALIBRATION CURVE FOR THIS EXPERIMENT.";POINTS
1820 CLS
1830 TEST = 1
1840 CALL OUTPUT(RELAY.MUX.01,TEST)
1850 DIM Z(POINTS,2), X(POINTS), Y(POINTS), C(100), D(100), KNOTS(POINTS,2), DEC
(16)
1860 '
1870 '
1880 ' OPEN DATA FILES
1890 '
1900 '
1910 TIMES = "00:00:00"
1920 COLOR 4
1930 LOCATE 14,18: PRINT "CREATING DATA FILES FOR CALIBRATION VOLTAGES"
1940 COLOR 1
1950 OPEN "HOTWIRE.DAT" FOR OUTPUT AS #1
1960 CLOSE #1
1970 TIME = VAL(RIGHT$(TIMES,2))
1980 IF TIME < 5 GOTO 1970 ELSE 1990
1990 '
2000 '
2010 ' START DATA ACQUISITION

```

```

2020 '
2030 '
2040 READING = 0: CHANNEL = 0
2050 FOR READING = 1 TO POINTS
2051   CLS: LOCATE 10,15: PRINT "DEPRESS BUTTON      ON THE PARASCIENTIFIC TRANSDU
CER"
2052   COLOR 4: LOCATE 10,30: PRINT "P1": COLOR 1
2020 '
2030 '
2040 READING = 0: CHANNEL = 0
2050 FOR READING = 1 TO POINTS
2051   CLS: LOCATE 10,15: PRINT "DEPRESS BUTTON      ON THE PARASCIENTIFIC TRANSDU
CER"
2052   COLOR 4: LOCATE 10,30: PRINT "P1": COLOR 1
2053   LOCATE 12,15: PRINT "MAKE SURE NO OTHER FUNCTION BUTTONS ARE DEPRESSED"
2054   COLOR 4: LOCATE 21,28: PRINT "PRESS ENTER TO CONTINUE"
2055   AS = INKEY$: IF AS = "" THEN 2055
2060   CLS: LOCATE 8,17: COLOR 1
2070   IF READING = 1 GOTO 2080 ELSE 2100
2080   PRINT "IS THE PROBE POSITIONED FOR YOUR FIRST READING?"
2090   GOTO 2110
2100   LOCATE 8,19: PRINT "IS THE PROBE POSITIONED FOR A NEW READING?"
2110   COLOR 4: LOCATE 9,36: INPUT "1 = YES";ANS5
2120   IF ANS5 <> 1 GOTO 2060
2130   COLOR 1
2140   CLS: LOCATE 16,19: COLOR 1: PRINT "IS THE TUNNEL SET FOR A NEW FLOW VELOC
ITY?"
2150   COLOR 4: LOCATE 17,36: INPUT "1 = YES";ANS6
2160   IF ANS6 <> 1 GOTO 2140
2170   CLS: COLOR 20: LOCATE 8,35: PRINT "STAND BY"
2180   COLOR 1: LOCATE 13,24: PRINT "DATA VALUES FOR HOT WIRE VOLTAGE"
2190   LOCATE 15,25: PRINT "AND TEST SECTION VELOCITY ARE"
2200   LOCATE 17,30: PRINT "NOW BEING COLLECTED"
2210   FOR CHANNEL = 1 TO 2
2220     ON CHANNEL GOTO 2230,2342
2230     CALL OUTPUT(RELAY.MUX.01,CHANNEL)
2240     CALL SET.RANGE(DMM.01,R20)
2250     I = 0: SUM1 = 0: FOR I = 1 TO 100
2260       IF I = 1 GOTO 2270 ELSE 2290
2270       TIME = .5
2280       CALL DELAY(TIME)
2290       CALL MEASURE(DMM.01,C(I))
2300       SUM1 = SUM1 + ABS(C(I))
2310     NEXT I
2320     AVG1 = SUM1/100
2330     Z(READING,CHANNEL) = AVG1
2340   GOTO 2780
2342     I = 0
2344     SUM2 = 0
2370     FOR I = 1 TO 100
2410       CALL MEASURE(DIG.IN.01,D(I))
2420       SUM2 = SUM2 + D(I)
2430     NEXT I
2440     DN = SUM2/100
2442     GOSUB 5480
2450     Z(READING,CHANNEL) = PRESS
2460     GOSUB 4270
2470     GOSUB 4700
2480     Z(READING,CHANNEL) = VEL
2490     KNOTS(READING,CHANNEL) = KTS

```

```

2500 BEEP: CLS: LOCATE 2,32: PRINT "CALIBRATION DATA"
2510 LOCATE 4,17: PRINT "HOT WIRE VOLTAGE"
2520 LOCATE 4,46: PRINT "WIND TUNNEL VELOCITY": COLOR 4
2530 LOCATE 6,19: PRINT USING "#.####";Z(READING,1): COLOR 1
2540 LOCATE 6,26: PRINT "VOLTS": COLOR 4
2550 LOCATE 6,41: PRINT USING "###.###";Z(READING,2): COLOR 1
2500 BEEP: CLS: LOCATE 2,32: PRINT "CALIBRATION DATA"
2510 LOCATE 4,17: PRINT "HOT WIRE VOLTAGE"
2520 LOCATE 4,46: PRINT "WIND TUNNEL VELOCITY": COLOR 4
2530 LOCATE 6,19: PRINT USING "#.####";Z(READING,1): COLOR 1
2540 LOCATE 6,26: PRINT "VOLTS": COLOR 4
2550 LOCATE 6,41: PRINT USING "###.###";Z(READING,2): COLOR 1
2560 LOCATE 6,49: PRINT "FT/SEC": COLOR 4
2570 LOCATE 6,58: PRINT USING "###.###";KNOTS(READING,2): COLOR 1
2580 LOCATE 6,66: PRINT "KNOTS": LOCATE 6,56: PRINT "="
2590 LOCATE 8,15: PRINT "THIS IS DATA POINT ";READING;" OF ";POINTS
2600 LOCATE 10,32: PRINT "WIND TUNNEL DATA"
2610 LOCATE 12,15: PRINT "TUNNEL TEMP ="
2620 COLOR 4: LOCATE 12,29: PRINT USING "##.##";TF: COLOR 1
2630 LOCATE 12,35: PRINT "DEG F"
2640 LOCATE 14,15: PRINT "TUNNEL STATIC PRESSURE ="
2650 COLOR 4: LOCATE 14,40: PRINT USING "####.###";PSTAT: COLOR 1
2660 LOCATE 14,48: PRINT "LB/FT^2"
2670 LOCATE 16,15: PRINT "TUNNEL AIR DENSITY ="
2680 COLOR 4: LOCATE 16,36: PRINT USING "#.#####";DENSITY: COLOR 1
2690 LOCATE 16,44: PRINT "LB/FT^3"
2700 LOCATE 18,15: PRINT "DYNAMIC PRESSURE ="
2710 COLOR 4: LOCATE 18,34: PRINT USING "##.##";Q: COLOR 1
2720 LOCATE 18,40: PRINT "LB/FT^2"
2730 IF READING = POINTS GOTO 2750
2740 COLOR 20: LOCATE 21,24: PRINT "SET NEW FLOW VELOCITY IN TUNNEL"
2750 COLOR 4: LOCATE 23,27: PRINT "PRESS ANY KEY TO CONTINUE"
2760 A$ = INKEY$: IF A$ = "" THEN 2760
2770 COLOR 1
2780 NEXT CHANNEL
2790 NEXT READING
2800 BNUM1 = Z(1,2)
2810 BNUM2 = Z(POINTS,2)
2820 BNUM3 = KNOTS(1,2)
2830 BNUM4 = KNOTS(POINTS,2)
2840 '
2850 '
2860 ' STORE DATA IN DATA FILE LABELED "HOTWIRE.DAT"
2870 '
2880 '
2890 CLS: LOCATE 8,15: PRINT "DATA VALUES ARE BEING STORED IN DATA FILE LABELED"

2900 COLOR 4: LOCATE 10,34: PRINT "HOTWIRE.DAT": COLOR 1
2910 I = 0: C1 = 0: C2 = 0: D1 = 0: D2 = 0
2920 FOR I = 1 TO POINTS
2930 X(I) = SQR(Z(I,2))
2940 Y(I) = (Z(I,1))^2
2950 C1 = C1 + X(I)
2960 C2 = C2 + X(I)^2
2970 D1 = D1 + Y(I)
2980 D2 = D2 + X(I)*Y(I)
2990 NEXT I
3000 OPEN "HOTWIRE.DAT" FOR APPEND AS #1
3010 J = 0: FOR J = 1 TO POINTS
3020 PRINT #1,USING"###.####";Y(J), X(J)

```

```

3030 NEXT J
3040 CLOSE #1
3050 '
3060 '
3070 ' SOLVE FOR SLOPE AND Y-INTERCEPT OF REGRESSION LINE
3080 '
3090 '
3030 NEXT J
3040 CLOSE #1
3050 '
3060 '
3070 ' SOLVE FOR SLOPE AND Y-INTERCEPT OF REGRESSION LINE
3080 '
3090 '
3100 A = (POINTS*D2-C1*D1)/(POINTS*C2-C1^2)
3110 IF ABS(A) < 1E-08 THEN A=0
3120 B = (D1-A*C1)/POINTS
3130 IF ABS(B) < 1E-08 THEN B=0
3140 '
3150 '
3160 ' PRINT SUMMARY OF CALIBRATION DATA ON SCREEN
3170 '
3180 '
3190 LOCATE 16,12: PRINT "WOULD YOU LIKE TO SEE A SUMMARY OF YOUR CALIBRATION DA
TA"
3200 LOCATE 18,33: PRINT "ON THE SCREEN?": COLOR 4
3210 LOCATE 20,27: INPUT "ENTER 1 FOR YES, 0 FOR NO";ANS7
3220 IF ANS7 <> 0 GOTO 3230 ELSE 3640
3230 COLOR 1: CLS: LOCATE 2,32: PRINT "CALIBRATION DATA"
3240 LOCATE 4,9: PRINT "HOT WIRE VOLTAGE (VOLTS)"
3250 LOCATE 4,41: PRINT "WIND TUNNEL VELOCITY (FT/SEC)": COLOR 4
3260 J = 0
3270 FOR J = 1 TO POINTS
3280     LOCATE J+5,18: PRINT USING"#.####";Z(J,1)
3290     LOCATE J+5,52: PRINT USING"###.###";Z(J,2)
3300 NEXT J
3310 '
3320 '
3330 ' SEND CALIBRATION DATA TO HP LASER JET PRINTER
3340 '
3350 '
3360 COLOR 1: LOCATE 22,20: PRINT "WOULD YOU LIKE A HARD COPY OF THIS DATA?"
3370 COLOR 4: LOCATE 23,27: INPUT "ENTER 1 FOR YES, 2 FOR NO";ANS8
3380 IF ANS8 <> 2 GOTO 3390 ELSE 3640
3390 CLS: LOCATE 12,26: PRINT "DATA SENT TO LASER PRINTER": COLOR 1
3400 TIMES = "00:00:00"
3410 TIME = VAL(RIGHT$(TIMES,2))
3420 IF TIME < 5 GOTO 3410 ELSE 3430
3430 LPRINT: LPRINT
3440 LPRINT TAB(32): LPRINT "CALIBRATION DATA"
3450 LPRINT
3460 LPRINT TAB(9): LPRINT "HOTWIRE VOLTAGE (VOLTS)           WIND TUNNEL VELO
CITY"
3470 LPRINT TAB(42): LPRINT "(FT/SEC)                   (KTS)"
3480 LPRINT
3490 J = 0
3500 FOR J = 1 TO POINTS
3510     LPRINT TAB(18);
3520     LPRINT USING"#.####";Z(J,1);
3530     LPRINT TAB(43);

```

```

3540 LPRINT USING"###.###";Z(J,2);
3550 LPRINT TAB(61);
3560 LPRINT USING"###.###";KNOTS(J,2)
3570 NEXT J
3580 LPRINT CHR$(12)
3590 '
3540 LPRINT USING"###.###";Z(J,2);
3550 LPRINT TAB(61);
3560 LPRINT USING"###.###";KNOTS(J,2)
3570 NEXT J
3580 LPRINT CHR$(12)
3590 '
3600 '
3610 ' PRINT VIEW PLOT OF CALIBRATION CURVE ON THE SCREEN
3620 '
3630 '
3640 COLOR 1: CLS: LOCATE 12,13: PRINT "WOULD YOU LIKE TO SEE A PLOT OF THE CALI
BRATION CURVE?"
3650 COLOR 4: LOCATE 14,27: INPUT "ENTER 1 FOR YES, 2 FOR NO";ANS9
3660 COLOR 1: IF ANS9 <> 2 GOTO 3670 ELSE 3730
3670 CLS: SHELL "COMMAND/C HOT1.BAT"
3680 '
3690 '
3700 ' SEND HARD COPY OF CALIBRATION CURVE TO HP LASER JET PRINTER
3710 '
3720 '
3730 COLOR 1: CLS: LOCATE 12,19: PRINT "WOULD YOU LIKE A HARD COPY OF THIS GRAPH
?"
3740 LOCATE 14,27: COLOR 4: INPUT "ENTER 1 FOR YES, 2 FOR NO";ANS10
3750 COLOR 1: IF ANS10 <> 2 GOTO 3760 ELSE 3840
3760 CLS: COLOR 1: LOCATE 10,21: PRINT "THIS PROGRAM WILL AUTOMATICALLY LEAVE"
3770 LOCATE 12,22: PRINT "BASICA AND ENTER A GRAPHICS PROGRAM."
3780 LOCATE 14,14: PRINT "THE PLOT TAKES APPROXIMATELY 4-6 MINUTES TO COMPLETE"
3790 COLOR 4: LOCATE 21,27: PRINT "PRESS ANY KEY TO CONTINUE"
3800 A$ = INKEY$: IF A$ = "" THEN 3800
3810 COLOR 1
3820 SHELL "HOT2.BAT"
3830 BEEP
3840 OPEN "CHAIN.DAT" FOR OUTPUT AS #1
3850 PRINT #1,USING"###.###"; A, B, BNUM1, BNUM2, BNUM3, BNUM4, TF
3860 CLOSE #1
3870 '
3880 '
3890 ' PRINT CONCLUDING SCREEN AND SUMMARY OF CALIBRATION RANGE
3900 '
3910 '
3920 CLS: LOCATE 8,14: PRINT "THIS CONCLUDES THE CALIBRATION CURVE PORTION OF YO
UR"
3930 LOCATE 10,10: PRINT "EXPERIMENT. THE HOT WIRE SYSTEM IS NOW ACCURATELY CALI
BRATED"
3940 LOCATE 12,13: PRINT "WITHIN A WIND TUNNEL VELOCITY RANGE OF"
3950 COLOR 4: LOCATE 12,52: PRINT USING"###.###";Z(1,2)
3960 LOCATE 12,61: PRINT "FT/SEC": COLOR 1
3970 LOCATE 14,17: PRINT "(" LOCATE 14,18: PRINT USING "###.###";KNOTS(1,2)
3980 LOCATE 14,26: PRINT "KTS) TO": COLOR 4
3990 LOCATE 14,34: PRINT USING "###.###";Z(POINTS,2): LOCATE 14,42: PRINT "FT/SE
C": COLOR 1: LOCATE 14,49: PRINT "("
4000 LOCATE 14,50: PRINT USING "###.###";KNOTS(POINTS,2)
4010 LOCATE 14,58: PRINT "KTS)"
4020 COLOR 4: LOCATE 20,24: PRINT "ENTER 1 TO CONTINUE, 2 TO ABORT"

```

```

4030 LOCATE 21,28: INPUT "OR 3 TO GO BACK ONE PAGE";ANS11
4040 ON ANS11 GOTO 4100,5950,3730
4050 '
4060 '
4070 ' PRINT LAST SCREEN AND CALIBRATION EQUATION
4080 '
4030 LOCATE 21,28: INPUT "OR 3 TO GO BACK ONE PAGE";ANS11
4040 ON ANS11 GOTO 4100,5950,3730
4050 '
4060 '
4070 ' PRINT LAST SCREEN AND CALIBRATION EQUATION
4080 '
4090 '
4100 CLS: LOCATE 8,30: PRINT "Y = "
4110 LOCATE 8,34: PRINT USING "##.###";A: LOCATE 8,40: PRINT "X"
4120 IF B>=0 THEN LOCATE 8,42: PRINT "+": LOCATE 8,44: PRINT USING "##.###";B EL
SE LOCATE 8,42: PRINT "-": LOCATE 8,44: PRINT USING "##.###";ABS(B)
4130 COLOR 1: LOCATE 10,10: PRINT "THIS IS THE STRAIGHT LINE EQUATION OF THE CAL
IBRATION CURVE"
4140 LOCATE 12,19: PRINT "IT WILL AUTOMATICALLY BE ENTERED IN PART 2"
4150 LOCATE 14,26: PRINT "OF YOUR HOT WIRE EXPERIMENT"
4160 COLOR 4: LOCATE 20,27: PRINT " ENTER 1 TO START PART TWO"
4170 LOCATE 21,32: PRINT "ENTER 2 TO ABORT"
4180 LOCATE 22,25: INPUT "OR ENTER 3 TO GO BACK ONE PAGE";ANS12
4190 COLOR 1
4200 ON ANS12 GOTO 4210,5950,3920
4210 LOAD "PART2",R
4220 '
4230 '
4240 ' SUBROUTINE FOR MEASURING WIND TUNNEL TEMPERATURE
4250 '
4260 '
4270 A1 = 38.709457#
4280 A2 = .037085566#
4290 A3 = 5.649552E-05
4300 B0 = .10086091#
4310 B1 = 25727.94369#
4320 B2 = -767345.8295#
4330 B3 = 78025595.81#
4340 B4 = -9247486589#
4350 B5 = 6.97688E+11
4360 B6 = -2.66192E+13
4370 B7 = 3.94078E+14
4380 B8 = 0
4390 B9 = 0
4400 REF.OUT = 8
4410 CALL OUTPUT(RELAY.MUX.01,REF.OUT)
4420 CALL ENABLE.OUTPUT(RELAY.MUX.01)
4430 CALL SET.FUNCTION(DMM.01,DCVOLTS)
4440 CALL SET.RANGE(DMM.01,R2)
4450 CALL DISABLE.INT.TRIGGER(DMM.01)
4460 COUNT = .5
4470 TIMES = "00:00:00"
4480 IF TIMER < COUNT GOTO 4480 ELSE 4490
4490 CALL MEASURE(DMM.01,V)
4500 TR = 100*V
4510 ER = (TR*(A1+TR*(A2+TR*A3)))*10^-6
4520 CALL SET.RANGE(DMM.01,R200MILLI)
4530 TC = 7
4540 CALL OUTPUT(RELAY.MUX.01,TC)

```

```

4550 COUNT = .5
4560 TIMES = "00:00:00"
4570 IF TIMER < COUNT GOTO 4570 ELSE 4580
4580 CALL MEASURE(DMM.01,ET)
4590 E = ER + ET
4600 Z = B5+E*(B6+E*(B7+E*(B8+E*B9)))
4550 COUNT = .5
4560 TIMES = "00:00:00"
4570 IF TIMER < COUNT GOTO 4570 ELSE 4580
4580 CALL MEASURE(DMM.01,ET)
4590 E = ER + ET
4600 Z = B5+E*(B6+E*(B7+E*(B8+E*B9)))
4610 T = B0+E*(B1+E*(B2+E*(B3+E*(B4+E*Z))))
4620 TF = (1.8*T) + 32
4630 RETURN
4640 '
4650 '
4660 ' SUBROUTINE FOR WIND TUNNEL DATA:
4670 '         STATIC PRESS IN TEST SECTION
4680 '         AIR DENSITY IN TEST SECTION
4690 '         DYNAMIC PRESSURE IN TEST SECTION
4700 '         TEST SECTION VELOCITY, FT/SEC AND KTS
4710 '
4720 '
4722 CLS: COLOR 1: LOCATE 10,15: PRINT "DEPRESS BUTTON      ON THE PARASCIENTIFIC
TRANSUCER"
4724 COLOR 4: LOCATE 10,30: PRINT "P2": COLOR 1
4726 LOCATE 12,15: PRINT "MAKE SURE NO OTHER FUNCTION BUTTONS ARE DEPRESSED"
4728 COLOR 4: LOCATE 21,28: PRINT "PRESS ENTER TO CONTINUE"
4730 A$ = INKEY$: IF A$ = "" THEN 4730
4800 CALL MEASURE(DIG.IN.01,DN)
4802 GOSUB 5480
4810 PSTAT = PRESS*144
4820 TTEMP = TF + 459.67
4830 GASCONST = 53.3
4840 DENSITY = PSTAT/(GASCONST*TTEMP)
4850 DELTAP = Z(READING,CHANNEL)*144
4860 Q = DELTAP/.93
4870 IF Q < 1.5 THEN Q = 0
4880 GC = 32.174
4890 VEL = SQR(ABS((2*Q*GC)/DENSITY))
4900 KTS = VEL * .5924
4910 RETURN
4920 '
4930 '
4940 ' SUBROUTINE FOR READING AOA
4950 '
4960 '
4970 INPUT.CH = 5
4980 CALL OUTPUT(RELAY.MUX.01,INPUT.CH)
4990 CALL ENABLE.OUTPUT(RELAY.MUX.01)
5000 TIME = 3
5010 CALL DELAY(TIME)
5020 CALL MEASURE(DMM.01,AOA)
5030 HAVEAOA = (AOA-.003)*1000/10
5040 RETURN
5050 '
5060 '
5070 ' SUBROUTINE FOR AOA SELECTION
5080 '

```

```

5090 '
5100 WHILE (CINT(ABS(WANTAOA - HAVEAOA) * 10) / 10) >= .25
5110   ABSDIFF = ABS(WANTAOA - HAVEAOA)
5120   IF ABSDIFF > 36 THEN ABSDIFF = 36
5130   SWITCH.1 = 1
5090 '
5100 WHILE (CINT(ABS(WANTAOA - HAVEAOA) * 10) / 10) >= .25
5110   ABSDIFF = ABS(WANTAOA - HAVEAOA)
5120   IF ABSDIFF > 36 THEN ABSDIFF = 36
5130   SWITCH.1 = 1
5140   SWITCH.2 = 2
5150   CALL OPEN.CHANNEL(RELAY.ACT.01,SWITCH.1)
5160   CALL OPEN.CHANNEL(RELAY.ACT.01,SWITCH.2)
5170   IF WANTAOA > HAVEAOA GOTO 5210 ELSE 5340
5180   '
5190   ' THIS PART OF THE SUBROUTINE MOVES THE TURNTABLE FORWARD
5200   '
5210   IF (CINT(ABSDIFF*10)/10) >= .4 THEN TIMING = 100 ELSE TIMING = 1
5220   COUNT = ((ABSDIFF * TIMING) + 190) / 1000
5230   IF COUNT > 3 THEN COUNT = 3
5240   CALL CLOSE.CHANNEL(RELAY.ACT.01,SWITCH.1)
5250   CALL DELAY(COUNT)
5260   CALL OPEN.CHANNEL(RELAY.ACT.01,SWITCH.1)
5270   TIME = .5
5280   CALL DELAY(TIME)
5290   GOSUB 4940
5300   GOTO 5440
5310   '
5320   ' THIS PART OF THE SUBROUTINE MOVES THE TURNTABLE IN REVERSE
5330   '
5340   IF (CINT(ABSDIFF*10)/10) >= .4 THEN TIMING = 100 ELSE TIMING = 1
5350   COUNT = ((ABSDIFF * TIMING) + 190)/1000
5360   IF COUNT > 3 THEN COUNT = 3
5370   CALL CLOSE.CHANNEL(RELAY.ACT.01,SWITCH.2)
5380   CALL DELAY(COUNT)
5390   CALL OPEN.CHANNEL(RELAY.ACT.01,SWITCH.2)
5400   TIME = .5
5410   CALL DELAY(TIME)
5420   GOSUB 4940
5430   GOTO 5440
5440 WEND
5450 RETURN
5460 '
5470 '
5480 ' SUBROUTINE FOR CONVERTING DECIMAL PRESSURE VALUES TO NUMERIC VALUES
5490 '
5500 '
5510 COUNT = 0: PRESS = 0
5520 '
5530 ' DN IS THE MEASURED DECIMAL NUMBER
5540 ' DEC IS THE DECIMAL TRANSFORM MATRIX
5550 ' PRESS IS THE CONVERTED NUMERIC PRESSURE VALUE
5560 '
5570 DEC(16) = 10: DEC(15) = 8: DEC(14) = 4: DEC(13) = 2: DEC(12) = 1
5580 DEC(11) = .8: DEC(10) = .4: DEC(9) = .2: DEC(8) = .1: DEC(7) = .08
5590 DEC(6) = .04: DEC(5) = .02: DEC(4) = .01: DEC(3) = 8.000001E-03
5600 DEC(2) = .004: DEC(1) = .002
5610 '
5620 IF DN < 0 THEN PRESS = DEC(16) ELSE GOTO 5640
5630 COUNT = -32768!

```

```
5640 IF (DN-COUNT)/16384 >= 1 THEN PRESS = PRESS + DEC(15) ELSE GOTO 5660
5650 COUNT = COUNT + 16384
5660 IF (DN-COUNT)/8192 >= 1 THEN PRESS = PRESS + DEC(14) ELSE GOTO 5680
5670 COUNT = COUNT + 8192
5680 IF (DN-COUNT)/4096 >= 1 THEN PRESS = PRESS + DEC(13) ELSE GOTO 5700
5690 COUNT = COUNT + 4096
5700 IF (DN-COUNT)/2048 >= 1 THEN PRESS = PRESS + DEC(12) ELSE GOTO 5720
5710 COUNT = COUNT + 2048
5720 IF (DN-COUNT)/1024 >= 1 THEN PRESS = PRESS + DEC(11) ELSE GOTO 5740
5730 COUNT = COUNT + 1024
5740 IF (DN-COUNT)/512 >= 1 THEN PRESS = PRESS + DEC(10) ELSE GOTO 5760
5750 COUNT = COUNT + 512
5760 IF (DN-COUNT)/256 >= 1 THEN PRESS = PRESS + DEC(9) ELSE GOTO 5780
5770 COUNT = COUNT + 256
5780 IF (DN-COUNT)/128 >= 1 THEN PRESS = PRESS + DEC(8) ELSE GOTO 5800
5790 COUNT = COUNT + 128
5800 IF (DN-COUNT)/64 >= 1 THEN PRESS = PRESS + DEC(7) ELSE GOTO 5820
5810 COUNT = COUNT + 64
5820 IF (DN-COUNT)/32 >= 1 THEN PRESS = PRESS + DEC(6) ELSE GOTO 5840
5830 COUNT = COUNT + 32
5840 IF (DN-COUNT)/16 >= 1 THEN PRESS = PRESS + DEC(5) ELSE GOTO 5860
5850 COUNT = COUNT + 16
5860 IF (DN-COUNT)/8 >= 1 THEN PRESS = PRESS + DEC(4) ELSE GOTO 5880
5870 COUNT = COUNT + 8
5880 IF (DN-COUNT)/4 >= 1 THEN PRESS = PRESS + DEC(3) ELSE GOTO 5900
5890 COUNT = COUNT + 4
5900 IF (DN-COUNT)/2 >= 1 THEN PRESS = PRESS + DEC(2) ELSE GOTO 5920
5910 COUNT = COUNT + 2
5920 IF (DN-COUNT) = 1 THEN PRESS = PRESS + DEC(1)
5930 RETURN
5940 STOP
5950 CLS: SYSTEM
5960 END
```

APPENDIX B

TURBULENCE MAPPING RESULTS

The combined results of the turbulence mapping were presented in Chapter III. Shown below are the individual graphs which represent the turbulence intensity and length scale data for the four turbulence-generating grids. Attention should be given to the scales of the graphs.

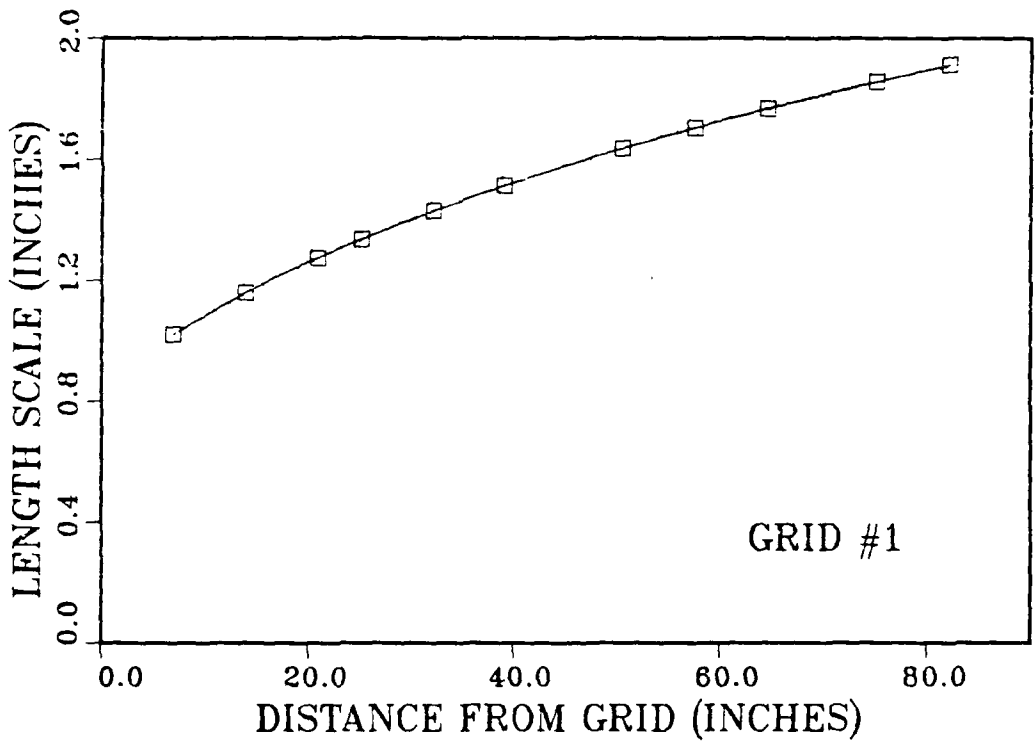
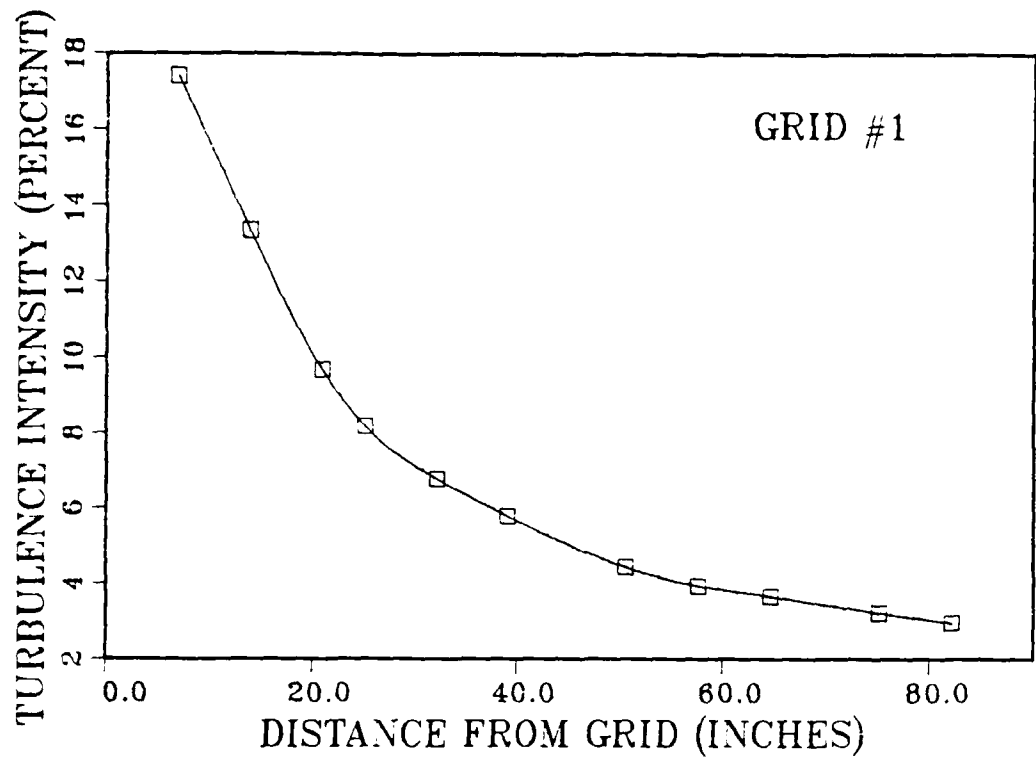


Figure B.1 Turbulence Intensities and Length Scales For Grid #1.

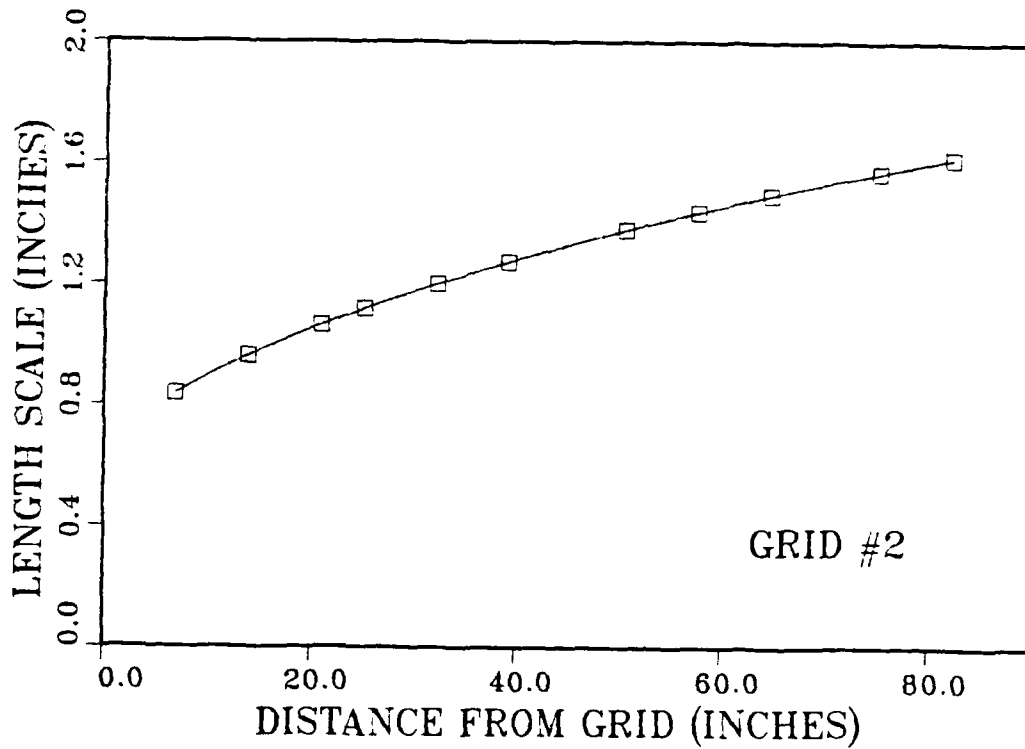
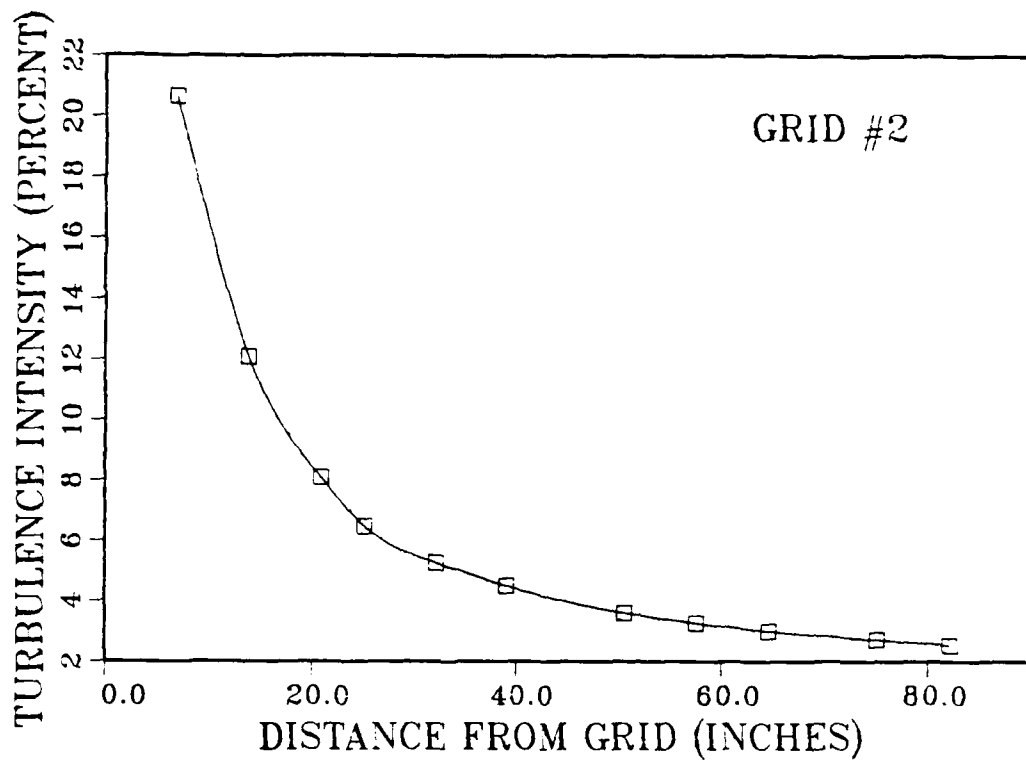


Figure B.2 Turbulence Intensities and Length Scales For Grid #2.

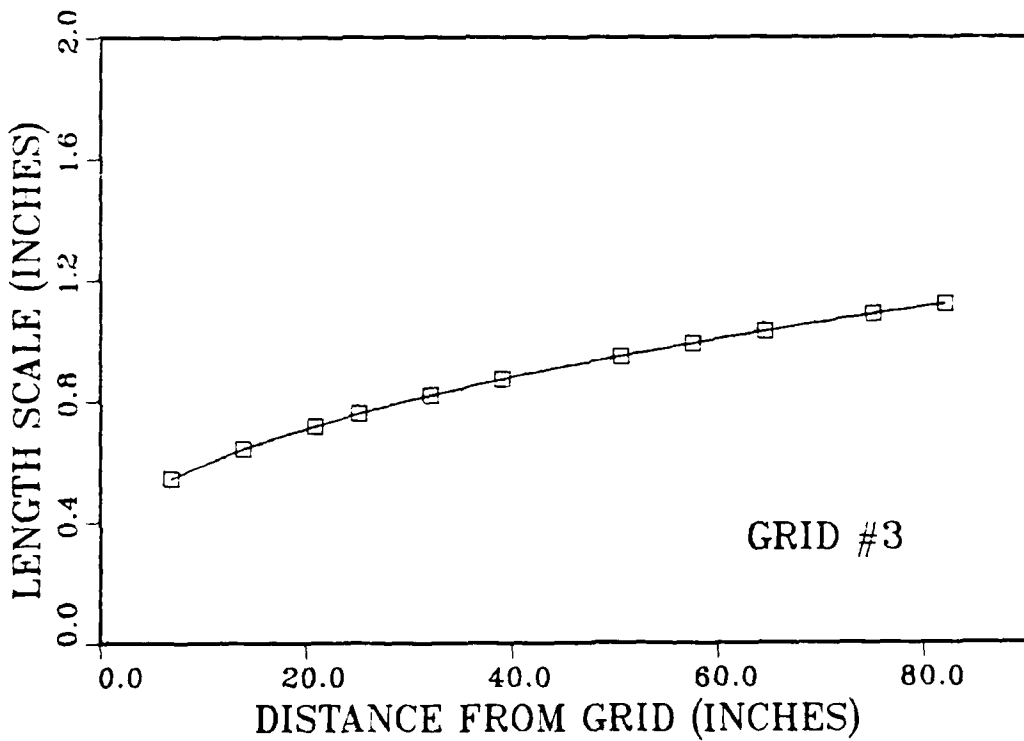
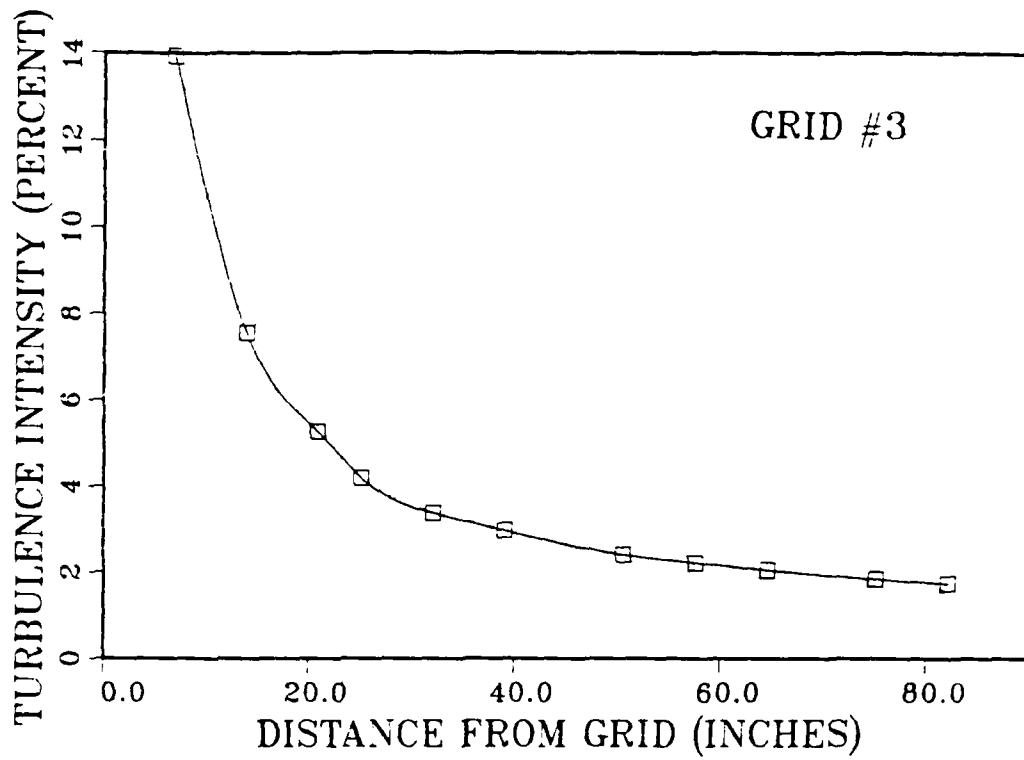


Figure B.3 Turbulence Intensities and Length Scales For Grid #3.

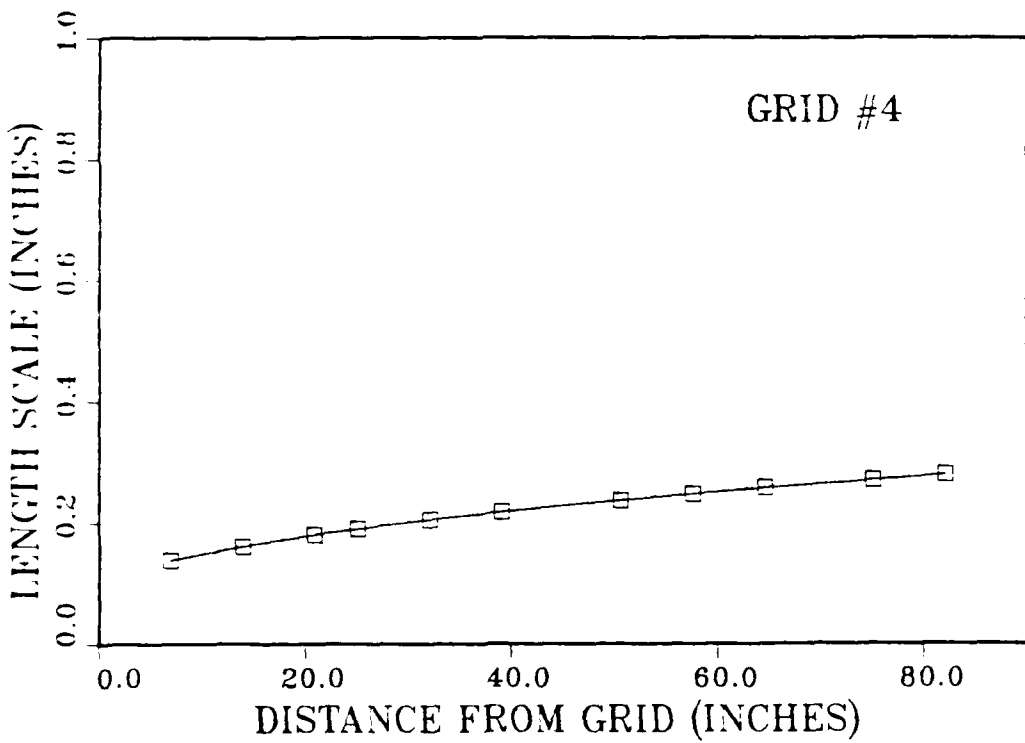
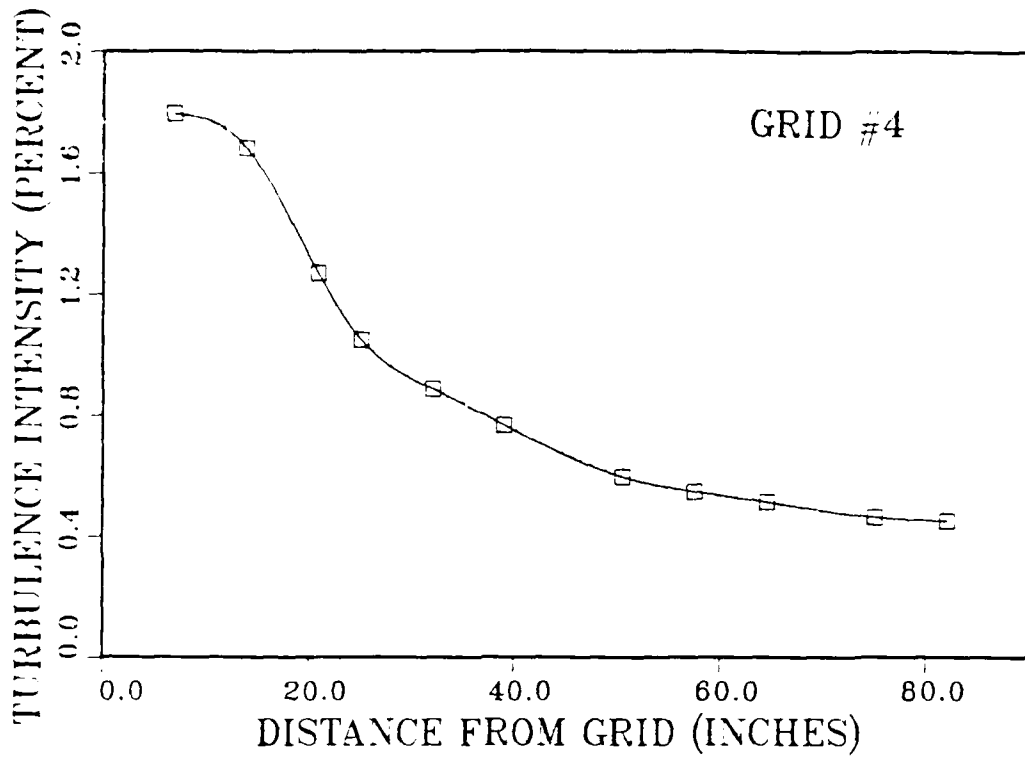


Figure B.4 Turbulence Intensities and Length Scales For Grid #4.

LIST OF REFERENCES

1. Tieleman, H. W., *A Survey of the Turbulence in the Marine Surface Layer for the Operation of Low-Reynolds Number Aircraft*, Virginia Polytechnic Institute and State University, Blacksburg, VA, March 1985.
2. Allen, H. J. and E. W. Perkins, *A Study of the Effects of Viscosity on Flow Over Slender Inclined Bodies of Revolution*, pp. 1103-1115, NACA TR 1048, 1951.
3. Thomson, K. D. and D. F. Morrison, *The Spacing, Position and Strength of Vortices in the Wake of Slender Cylindrical Bodies at Large Incidence*, Journal of Fluid Mechanics, Volume 50, Part 4, 1971.
4. Ericsson, L. E., and J. P. Reding, *Steady and Unsteady Vortex-Induced Asymmetric Loads on Slender Vehicles*, Journal of Spacecraft, Volume 18, Number 2, March-April 1981.
5. Dahlem, Valentine and Jack I. Flaherty, Christian E. G. Prziembel, Donald E. Shereda, *High Angle of Attack Missile Aerodynamics at Mach Numbers 0.30 to 1.5*, Technical Report AFWAL-TR-80-3070, November 1980.
6. Gregoriou, Gregor, *Modern Missile Design For High Angle-of-Attack*, AGARD Lecture Series 121, December 1982.
7. Keener, Earl R. and Gary T. Chapman, *Onset of Aerodynamic Side Forces at Zero Sideslip on Symmetric Forebodies at High Angles of Attack*, AIAA Paper 74-770, 1974.
8. Paul, Bernard P., *An Investigation of the Flow About an Ogive Cylinder at High Angles of Incidence*, Von Karman Institute for Fluid Dynamics, Project Report 1981-21, June 1981.
9. Ericsson, L. E., and J. P. Reding, *Alleviation of Vortex-Induced Asymmetric Loads*, Journal of Spacecraft, Volume 17, Number 6, November-December 1980.
10. Bradshaw, P., *An Introduction to Turbulence and its Measurement*, Pergamon Press, 1971.
11. Hancock, P. E. and P. Bradshaw, *The Effect of Free-Stream Turbulence on Turbulent Boundary Layers*, pp. 284-289, Journal of Fluids Engineering, Volume 105, September 1983.

12. Meier, H. U. and H.-P. Kreplin, *Influence of Freestream Turbulence on Boundary-Layer Development*, pp. 11-15, AIAA Journal, Volume 18, Number 1, January 1980.
13. Meteorological Office, *Handbook of Aviation Meteorology*, Her Majesty's Stationery Office, London, 1971.
14. Healey, J. Val, *Simulating the Helicopter-Ship Interface as an Alternative to Current Methods of Determining the Safe Operating Envelopes*, Naval Postgraduate School, Report NPS67-86-003, Monterey, CA, September, 1986.
15. Prizrembel, C. E. G. and Donald E. Shereda, *Aerodynamics of Slender Bodies at High Angles of Attack*, pp. 10-14, Journal of Spacecraft, Volume 16, Number 1, February 1979.
16. Farley, Harry D. (Jr.), Naval Sea Systems Command, Arlington, VA, private correspondence with author dated 20 April 1987.
17. Department of Aeronautics, *Laboratory Manual For Low-Speed Wind Tunnel Testing*, Naval Postgraduate School, Monterey, CA, October 1983.
18. Castro, I. P., *Effects of Free Stream Turbulence on Low Reynolds Number Boundary Layers*, Transactions of the ASME, Volume 106, September 1984.
19. Doremus, Gregory J., *Flowfield Measurements Using Hot-Wire Anemometry*, Master's Thesis, Naval Postgraduate School, Monterey, CA, September 1987.
20. Meier, H. U., *The Response of Turbulent Boundary Layers to Small Turbulence Levels in the External Free Stream*, ICAS Paper No. 76-05, October 1976.

INITIAL DISTRIBUTION LIST

		No. Copies
1.	Defense Technical Information Center Cameron Station Alexandria, VA 22304-6145	2
2.	Library, Code 0142 Naval Postgraduate School Monterey, CA 93943-5002	2
3.	Chairman Department of Aeronautics, Code 67 Naval Postgraduate School Monterey, CA 93943-5000	2
4.	Commander Naval Sea Systems Command SEA 62Z31 Washington, D.C. 20361-5001	5
5.	Commander Naval Surface Warfare Center Code G20 Dahlgren, VA 22448	5
6.	RADM D. P. Roane, USN (Ret.) P.O. Box 360 Dutton, VA 23050	1
7.	Prof. R. M. Howard Department of Aeronautics, Code 67Ho Naval Postgraduate School Monterey, CA 93943-5000	10
8.	Prof. J. V. Healey Department of Aeronautics, Code 67He Naval Postgraduate School Monterey, CA 93943-5000	1
9.	LT D. P. Roane, Jr., USN SWOSCOLCOM Dept. Head Class 102 Bldg. 446, NETC Newport, RI 02841	2

END

DATE

FILMED

6-88

DTIC